


Partial-wave analysis of $J/\psi \rightarrow \gamma\gamma\phi$

M. Ablikim *et al.**
(BESIII Collaboration)

 (Received 5 February 2025; accepted 11 March 2025; published 25 March 2025)

Using a sample of $\sim 10^{10}$ J/ψ events collected by the BESIII detector at the BEPCII collider, a partial-wave analysis of the decay $\gamma\gamma\phi$ is performed to investigate the intermediate resonances in $J/\psi \rightarrow \gamma R$, $R \rightarrow \gamma\phi$. Resonances including $f_1(1285)$, $\eta(1405)$, $f_1(1420)$, $f_1(1510)$, $f_2(1525)$, $X(1835)$, $f_2(1950)$, $f_2(2010)$, $f_0(2200)$, and η_c have been detected with statistical significance greater than 5σ . The product branching fractions $\mathcal{B}(J/\psi \rightarrow \gamma R, R \rightarrow \gamma\phi)$ are reported, and the resonance parameters of $\eta(1405)$ and $X(1835)$ have been precisely determined. It seems likely that $\eta(1405)$ and $X(1835)$ act as the first—and second—excited states of η' , respectively. The observation of $\eta_c \rightarrow \gamma\phi$ holds great significance for the in depth study of charmonium properties. No evidence of $\eta(1295)$, $\eta_1(1855)$ or $X(2370)$ is found. The measured upper limits of relevant branching fraction products do not conflict with theoretical expectations for $X(2370)$ as a pseudoscalar glueball and $\eta_1(1855)$ as a hybrid state.

DOI: [10.1103/PhysRevD.111.052011](https://doi.org/10.1103/PhysRevD.111.052011)

I. INTRODUCTION

The non-Abelian nature of quantum chromodynamics (QCD) predicts the existence of various exotic states, including glueballs, hybrids, and multiquark states [1]. Confirming these states experimentally would provide crucial insights into the confinement regime of QCD and serve as a direct test of QCD theory. Radiative decays of charmonium are glue-rich processes and serve as excellent probes for investigating the production of gluonic matter and light hadron structures [2]. While significant progress has been made in the past few decades [3], numerous unresolved issues persist.

One of the current focal points is the nature of the two pseudoscalar states around $1.4 \text{ GeV}/c^2$ [1], namely, the $\eta(1405)$ and $\eta(1475)$ as listed by the Particle Data Group (PDG) [4]. The $\eta(1475)$ is considered a potential first radial excitation of the η' , while the $\eta(1405)$ has been suggested as a candidate for the ground state pseudoscalar glueball [5,6]. However, the mass of $\eta(1405)$ is relatively far from the predicted mass of a pseudoscalar glueball ($2.3\text{--}2.6 \text{ GeV}/c^2$) by lattice QCD [7,8], leading to the long standing “E- η puzzle” [9]. It is still controversial whether the $\eta(1405)$ and $\eta(1475)$ are two separate states or just one pseudoscalar state observed in different decay modes.

The $X(1835)$ was first observed in the decay $J/\psi \rightarrow \gamma\pi^+\pi^-\eta'$ by BESII [10], with its spin-parity quantum numbers established as $J^{PC} = 0^{-+}$ by BESIII [11]. This discovery led to various theoretical speculations regarding its nature, including proposals such as $N\bar{N}$ bound state [12], a baryonium with a sizable gluon content [13], a second radial excitation of the η' [14,15], an η_c -glueball hybrid, and a pseudoscalar glueball [16]. So far, none of these interpretations has been ruled out or confirmed.

The $X(2370)$ has also been observed in the $J/\psi \rightarrow \gamma\pi^+\pi^-\eta'$ [17,18]. Recently, the BESIII experiment confirmed that the spin-parity of the $X(2370)$ as 0^{-+} via the decay $J/\psi \rightarrow \gamma K_S^0 K_S^0 \eta$ [19]. This experimental finding has prompted numerous theoretical speculations regarding its nature [14,20–23], with one fascinating hypothesis being a pseudoscalar glueball [8,24–27]. By using the radiative pseudoscalar glueball decay width, which is approximately $\Gamma_{PS \rightarrow \gamma\phi} \sim 95 \text{ keV}$, the total pseudoscalar glueball decay width is approximately $\Gamma_{PS} \sim 470 \dots 614 \text{ MeV}$ [28], and the branching fraction (BF) of J/ψ radiatively decaying into pseudoscalar glueball being $2.31(80) \times 10^{-4}$ [6], it can be deduced that if the $X(2370)$ is a pseudoscalar glueball, the $\mathcal{B}(J/\psi \rightarrow \gamma X(2370) \rightarrow \gamma\gamma\phi)$ should be less than 10^{-8} .

Recently, the BESIII collaboration reported the first observation of a $I^G(J^{PC}) = 0^+(1^{-+})$ structure $\eta_1(1855)$ through a partial-wave analysis (PWA) of the $J/\psi \rightarrow \gamma\eta\eta'$ decay [29], sparking a variety of theoretical interpretations, including hybrids [30–32], molecular states [33,34], and tetraquark states [35,36]. When considering the $\eta_1(1855)$ as an $s\bar{s}g$ hybrid, the total decay width is predicted to be approximately 160 MeV [37], and the radiative decay width $\Gamma_{\eta_1(1855) \rightarrow \gamma\phi} \sim 4.2 \times 10^{-2}$ [38]. Given that the BF for

*Full author list given at the end of the article.

Published by the American Physical Society under the terms of the [Creative Commons Attribution 4.0 International license](https://creativecommons.org/licenses/by/4.0/). Further distribution of this work must maintain attribution to the author(s) and the published article's title, journal citation, and DOI. Funded by SCOAP³.

the $J/\psi \rightarrow \gamma\eta_1(1855)$ decay is on the order of 10^{-5} [39], the BF $\mathcal{B}(J/\psi \rightarrow \gamma\eta_1(1855), \eta_1(1855) \rightarrow \gamma\phi)$ should be less than 10^{-9} .

Since radiative decays do not change the flavor structure, the decays $J/\psi \rightarrow \gamma R, R \rightarrow \gamma V$ with $V \equiv \rho, \omega, \phi$, serve as flavor filter reactions and play an important role in unraveling the quark contents of the intermediate resonances [40,41]. Throughout the text, the symbol R denotes intermediate resonance. Previously, the BESIII collaboration has studied the prominent features of $f_1(1285)$, $\eta(1475)$, and $X(1835)$ using 1.3 billion J/ψ events [42]. A one-dimensional fit to the $\gamma\phi$ invariant mass [$M(\gamma\phi)$] distribution from $J/\psi \rightarrow \gamma\gamma\phi$ was performed. In addition, from the angular distribution it was found that the data favors spin and parity (J^{PC}) assignments of 0^{-+} for the structures around $1.4 \text{ GeV}/c^2$ and $1.8 \text{ GeV}/c^2$.

Using a dataset of $(10087 \pm 44) \times 10^6$ J/ψ [43] events from e^+e^- annihilation data collected at the center-of-mass (c.m.) energy $\sqrt{s} = 3.097 \text{ GeV}$ with the BESIII detector at the BEPCII collider, we present the results of a PWA of $J/\psi \rightarrow \gamma\gamma\phi$ to extract the contributions of intermediate components and determining their spin-parity, mass, and width. The research results will provide useful information to help us understand the properties of $\eta(1405/1475)$ and $X(1835)$.

II. BESIII DETECTOR AND MC SAMPLE

The BESIII detector [44] records symmetric e^+e^- collisions from the BEPCII storage ring [45] in the c.m. energy range from 1.84 to 4.95 GeV, achieving a peak luminosity of $1.1 \times 10^{33} \text{ cm}^{-2} \text{ s}^{-1}$ at $\sqrt{s} = 3.773 \text{ GeV}$. BESIII has collected large data samples in this energy region [6,46,47]. The cylindrical core of the BESIII detector covers 93% of the full solid angle and includes a helium-based multilayer drift chamber (MDC), a plastic scintillator time-of-flight system (TOF), and a CsI(Tl) electromagnetic calorimeter (EMC), which are all enclosed in a superconducting solenoidal magnet providing a 1.0 T magnetic field. The magnetic field was 0.9 T in 2012, which affects 10.8% of the total J/ψ data. The end cap TOF system was upgraded in 2015, affecting 87.0% of the data used in this analysis [48]. A detailed description of the BESIII detector design and performance can be found in Ref. [44].

Simulated data samples, generated with a Geant4-based [49] Monte Carlo (MC) package, that includes the geometric description of the BESIII detector and the detector response [50], are utilized to determine detection efficiencies and estimate backgrounds. The simulation includes modeling of the beam energy spread and initial state radiation in the e^+e^- annihilations using the generator KKMC [51]. Signal MC samples of the process $\gamma\gamma\phi$ with the subsequent decays $\phi \rightarrow K^+K^-$ are generated uniformly in phase space (PHSP). The inclusive MC sample includes

both the production of the J/ψ resonance and the continuum processes incorporated in KKMC. All particle decays are modeled with EvtGen [52] using BFs either taken from the PDG [4], when available, or otherwise estimated with LUNDCHARM [53]. Final state radiation from charged final state particles is incorporated using the PHOTOS package [54].

III. EVENT SELECTION

Charged tracks detected in the MDC are required to be within a polar angle (θ) range of $|\cos\theta| < 0.93$, where θ is defined with respect to the z -axis, the symmetry axis of the MDC. The distance of closest approach to the interaction point (IP) must be less than 10 cm along the z -axis and less than 1 cm in the transverse plane. Particle identification for charged tracks combines measurements of the dE/dx in the MDC and the flight time in the TOF to form likelihoods $\mathcal{L}(h)$ ($h = p, K, \pi$) for each hadron h hypothesis. A track is identified as a kaon if its kaon hypothesis likelihood satisfies $\mathcal{L}(K) > \mathcal{L}(\pi)$ and $\mathcal{L}(K) > \mathcal{L}(p)$.

Photon candidates are identified by the showers produced in the EMC. The deposited energy of each shower must be larger than 25 MeV in the barrel region ($|\cos\theta| < 0.80$) and larger than 50 MeV in the end cap regions ($0.86 < |\cos\theta| < 0.92$). To exclude showers that originate from charged tracks, the angle subtended by the position of EMC shower [55] and the position of the closest charged track at the EMC as measured from the IP must be greater than 10 degrees as measured from the IP. To suppress electronic noise and showers unrelated to the event, the difference between the EMC time and the event start time is required to be within [0, 700] ns. Candidate events are required to have two oppositely charged tracks identified as kaons and have at least two photons.

A four-constraint (4C) kinematic fit is performed under the $J/\psi \rightarrow \gamma\gamma K^+K^-$ hypothesis for all combinations with good photon candidates. For events with more than one combination of $J/\psi \rightarrow \gamma\gamma K^+K^-$, only the combination with the minimum $\chi_{4C,2\gamma K^+K^-}^2$ is retained. Moreover, the $\chi_{4C,2\gamma K^+K^-}^2$ is required to be less than 40. To further suppress backgrounds from processes with one or three or four photons in the final state, 4C kinematic fits are performed under the hypotheses $J/\psi \rightarrow \gamma K^+K^-$, $J/\psi \rightarrow 3\gamma K^+K^-$ and $J/\psi \rightarrow 4\gamma K^+K^-$. The $\chi_{4C,2\gamma K^+K^-}^2$ is required to be less than all possible $\chi_{4C,\gamma K^+K^-}^2$, $\chi_{4C,3\gamma K^+K^-}^2$ and $\chi_{4C,4\gamma K^+K^-}^2$.

After the initial event selection, the $M(K^+K^-)$ distribution is shown in Fig. 1(a). The ϕ candidates are identified by requiring $|M(K^+K^-) - M_\phi| < 0.005 \text{ GeV}/c^2$, where M_ϕ is ϕ nominal mass. Figure 1(b) shows the $M(\gamma\gamma)$ distribution in the ϕ signal region, in which clear peaks corresponding to π^0 , η , and η' can be seen. To eliminate backgrounds involving $\pi^0 \rightarrow \gamma\gamma$, $\eta \rightarrow \gamma\gamma$, or $\eta' \rightarrow \gamma\gamma$ decays, events with $M(\gamma\gamma)$ within the ranges $M(\gamma\gamma) \in (0.11, 0.16) \text{ GeV}/c^2$,

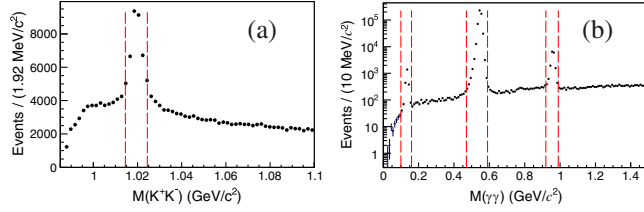


FIG. 1. Distributions of (a) $M(K^+K^-)$ and (b) $M(\gamma\gamma)$ with $M(K^+K^-)$ in the ϕ mass window of the accepted $J/\psi \rightarrow \gamma\gamma\phi$ candidate events in data, where the pair of red dashed vertical lines in the left figure denote the ϕ signal region, while the pairs of red dashed vertical lines in the right figure denote the π^0 , η or η' background regions.

$M(\gamma\gamma) \in (0.46, 0.59) \text{ GeV}/c^2$ or $M(\gamma\gamma) \in (0.92, 0.99) \text{ GeV}/c^2$ are excluded.

Despite these mass window constraints, the backgrounds from $J/\psi \rightarrow \phi\pi^0$, $J/\psi \rightarrow \phi\eta$, $J/\psi \rightarrow \phi\eta'$ cannot be entirely eliminated due to their tails. We try to quantify residual backgrounds using an inclusive MC sample. Figure 2(a), from this sample, depicts the Dalitz plot of $M^2(\gamma_{\text{high}}\phi)$ versus $M^2(\gamma_{\text{low}}\phi)$, where γ_{low} and γ_{high} refer to the photons with lower and higher energies in J/ψ rest frame. Notably, Fig. 2(a) reveals that these events cluster at the high end of the Dalitz plot. By imposing the condition $M^2(\gamma_{\text{high}}\phi) < 9 \text{ GeV}^2/c^4$ on data sample, these backgrounds can be effectively suppressed.

After applying all selection criteria to the data, the Dalitz plot of $M^2(\gamma_{\text{high}}\phi)$ versus $M^2(\gamma_{\text{low}}\phi)$ of the accepted $J/\psi \rightarrow \gamma\gamma\phi$ candidate events of data is depicted in Fig. 2(b). Subsequently, 38,383 events survive the event selection criteria.

IV. BACKGROUND TREATMENT

To quantify the contributions of ϕ -events and non- ϕ -events in the ϕ signal region, directly influencing the purity of the ϕ sample used in subsequent analyses, a one-dimensional fit to the $M(K^+K^-)$ distribution is performed, as shown in Fig. 3. In the fit, the signal is modeled by a relativistic P-wave Breit-Wigner (BW) function convolved with a Gaussian function describing the resolution

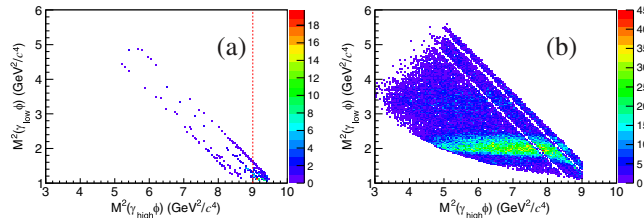


FIG. 2. (a) Dalitz plot of $M^2(\gamma_{\text{high}}\phi)$ versus $M^2(\gamma_{\text{low}}\phi)$ for the residual background events of $J/\psi \rightarrow \phi\pi^0$, $J/\psi \rightarrow \phi\eta$, $J/\psi \rightarrow \phi\eta'$ using the inclusive MC. (b) Dalitz plot of $M^2(\gamma_{\text{high}}\phi)$ versus $M^2(\gamma_{\text{low}}\phi)$ of data following all selection criteria.

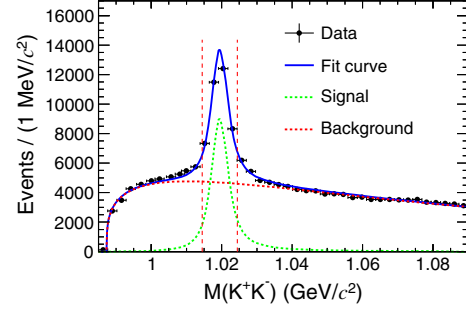


FIG. 3. The one-dimensional fit to the $M(K^+K^-)$ distribution. The dots with error bars are data, the blue line denotes the fit curve, the green dash line denotes the signal shape, the red dash line is background shape, and the pair of the red dashed vertical lines denote the ϕ signal region.

difference between data and MC simulation. The relativistic P-wave Breit-Wigner function is expressed as

$$BW(m) = \frac{F_m}{m_0^2 - m^2 - im_0\Gamma(m)}, \quad (1)$$

where F_m is the Blatt-Weisskopf damping factor $F_m = \sqrt{1 + (Rq_0)^2} / \sqrt{1 + (Rq)^2}$, R is fixed to 1.5 GeV^{-1} , and

$$\Gamma(m) = \Gamma(m_0) \left(\frac{q}{q_0}\right)^{2L+1} \left(\frac{m_0}{m}\right) F_m^2. \quad (2)$$

Here m_0 is the ϕ nominal mass from the PDG, q is momentum of either K^+ or K^- in the ϕ rest frame and q_0 is q evaluated at $m = m_0$.

The background shape is parametrized by a low- x cutoff function,

$$f(x, m_0, c, p) = x \cdot \left[\left(\frac{x}{m_0}\right)^2 - 1 \right]^p \cdot \exp \left[c \cdot \left(\left(\frac{x}{m_0}\right)^2 - 1 \right) \right]. \quad (3)$$

Here, x represents the observable $M(K^+K^-)$, with $m_0 = 0.987354$ denoting the threshold for two kaons, while c and p are free parameters in the fit.

Finally, the fractions of ϕ -events and non- ϕ -events are determined to be 55.3% and 44.7% in ϕ signal region, respectively. With the event selection criteria mentioned above, the residual backgrounds are classified into two categories: backgrounds without ϕ and backgrounds with ϕ . The handling methods for these two types of backgrounds are as follows.

A. Treatment of non- ϕ background

The dominant non- ϕ background components are mainly from $J/\psi \rightarrow \gamma R$ [$R = f_1(1285)$, $\eta(1405)$ and $f_1(1420)$], $R \rightarrow K^+K^-\pi^0$, with the $\gamma K^+K^-\pi^0$ final state. It is difficult to distinguish the signal from these

background components because the $M(K^+K^-)$ value from $R \rightarrow K^+K^-\pi^0$ is close to the K^+K^- mass threshold.

Based on the analysis of the signal-to-background ratio Q in the available PHSP around each specific event, the quality factor method [56] is used to estimate the non- ϕ backgrounds. For this procedure, we need to know the functional dependence of the signal and background distributions in terms of a distinct kinematic variable (ζ_r). The first step is to assign a number of n_c nearest neighbors for each event including the event itself. In order to measure distances between events, a collection of kinematic observables ($\vec{\zeta}$) that span the PHSP for the reaction is selected to define a metric. Using this metric, the distance between any two events, d_{ij} , is given as

$$d_{ij}^2 = \sum_k \left[\frac{\zeta_k^i - \zeta_k^j}{\Delta_k} \right]^2, \quad (4)$$

where the sum is over all kinematic observables ($\vec{\zeta}$), and Δ_k is a normalization factor that represents the weight of the kinematic variable.

The n_c nearest neighbors are then fit with the unbinned maximum likelihood method, with estimators written as

$$f(\zeta_r) = f_s \cdot S(\zeta_r) + (1 - f_s) \cdot B(\zeta_r), \quad (5)$$

where $S(\zeta_r)$ and $B(\zeta_r)$ represent the probability density functions of signal and background, respectively, and f_s describes a signal fraction with a value constrained within the range [0.0, 1.0]. The Q-value for each event is then given by

$$Q = \frac{f_s \cdot S(\zeta_r)}{f_s \cdot S(\zeta_r) + (1 - f_s) \cdot B(\zeta_r)}, \quad (6)$$

in which Q and (1-Q) represent the probabilities of an event to be signal and background, respectively, which are used as an event-weight to determine the contribution of the signal to a given physical distribution.

In this analysis, seven coordinates are chosen for the metric, which are presented in Table I. Throughout this paper, the polar angle is denoted by θ , while the azimuth is represented by φ . It is necessary to make the value of n_c as small as possible. This is to ensure that the phase space (PHSP) cell of all the selected neighbors remains small and that the background varies smoothly within the cell. However, n_c also has to be large enough to guarantee stable and reliable fits to $M(K^+K^-)$. Through the study of the Monte Carlo (MC) samples, we have reached the conclusion that setting $n_c = 200$ will result in an appropriate size.

For this analysis, $M(K^+K^-)$ is chosen as the distinct kinematic variable. The fitting model of $M(K^+K^-)$ is the same as the fit mentioned earlier. As a result, the angular

TABLE I. Set of the kinematic observables ($\vec{\zeta}_k$) used for background subtraction.

$\vec{\zeta}_k$	Description	Δ_k
$\cos \theta_{\gamma_{\text{high}}}$	Cosine of polar angle of the high-energy photon in the rest frame of J/ψ	2
$\cos \theta_{K^+}$	Cosine of polar angle of K^+ in the rest frame of ϕ	2
$\cos \theta_{\phi}$	Cosine of polar angle of ϕ in the rest frame of $\gamma_{\text{low}}\phi$	2
φ_{K^+}	Azimuth of K^+ in the rest frame of ϕ	2π
φ_{ϕ}	Azimuth of ϕ in the rest frame of $\gamma_{\text{low}}\phi$	2π
$M^2(\gamma_{\text{low}}\phi)$	Invariant mass squared of $\gamma_{\text{low}}\phi$	$0.1 \text{ GeV}^2/c^4$
$M^2(\gamma_{\text{high}}\phi)$	Invariant mass squared of $\gamma_{\text{high}}\phi$	$0.15 \text{ GeV}^2/c^4$

distributions and several invariant mass spectra of the selected events within the ϕ signal region with Q-weighted and (1-Q)-weighted are shown in Fig. 4. The sum of all obtained Q-values (weights) is taken as the number of signal events, yielding 20,453 events. All further analysis steps are performed using this weighted data sample.

B. Treatment of ϕ background

The dominant ϕ related background is $J/\psi \rightarrow \phi\pi^0\pi^0$, which includes intermediate resonances [57]. A multidimensional reweighting method [58] is applied to the PHSP MC sample to obtain a ‘‘datalike’’ MC sample of $J/\psi \rightarrow \phi\pi^0\pi^0$. Figure 5 shows the comparison of some typical kinematic variables of data and weighted PHSP MC sample of the selected $J/\psi \rightarrow \phi\pi^0\pi^0$ candidate events. These indicate good consistency between data and MC simulation. Here π_1^0 and π_2^0 denote the π^0 s with higher and lower energies in the $\phi\pi^0\pi^0$ final state, respectively. The estimated MC events of $J/\psi \rightarrow \phi\pi^0\pi^0$ are subjected to the selection criteria of $J/\psi \rightarrow \gamma\gamma\phi$. The surviving events are normalized according to the BF, as depicted in Fig. 4. This process yields 3155 background events, which are subsequently subtracted by assigning negative weights in the PWA.

The surviving background events $J/\psi \rightarrow \phi\pi^0$, $J/\psi \rightarrow \phi\eta$ and $J/\psi \rightarrow \phi\eta'$ are normalized according to the PDG BFs [4], resulting in 157 background events which also will be subtracted from the data by assigning negative weights to them in the PWA.

V. PARTIAL-WAVE ANALYSIS

Using the GPUPWA framework [59], a PWA is performed on the selected candidate events of $\gamma\gamma\phi$, $\phi \rightarrow K^+K^-$, to disentangle the structures in the Dalitz plot. The amplitudes in the sequential radiative decay $J/\psi \rightarrow \gamma R$, $R \rightarrow \gamma\phi$ are constructed using the covariant

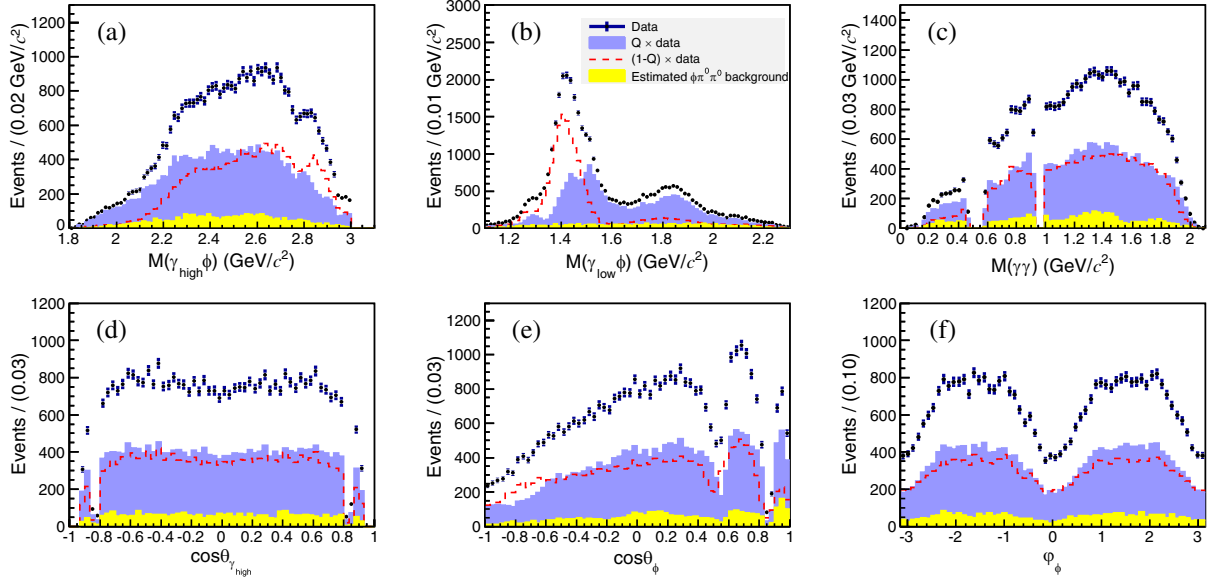


FIG. 4. Distributions of (a) $M(\gamma_{\text{high}}\phi)$, (b) $M(\gamma_{\text{low}}\phi)$, (c) $M(\gamma\gamma)$, (d) cosine of the polar angle of γ_{high} , (e) cosine of the polar angle of ϕ in $\gamma_{\text{low}}\phi$, and (f) azimuth of ϕ of the accepted $J/\psi \rightarrow \gamma\gamma\phi$ candidate events. The black dots with error bars are the selected events in the ϕ signal region without any weight, the purple shaded regions are Q -weighted data, and the red dashed lines are $(1-Q)$ weighted data. The yellow shadowed regions are the estimated MC events of $J/\psi \rightarrow \phi\pi^0\pi^0$ that have passed the selection criteria of $J/\psi \rightarrow \gamma\gamma\phi$.

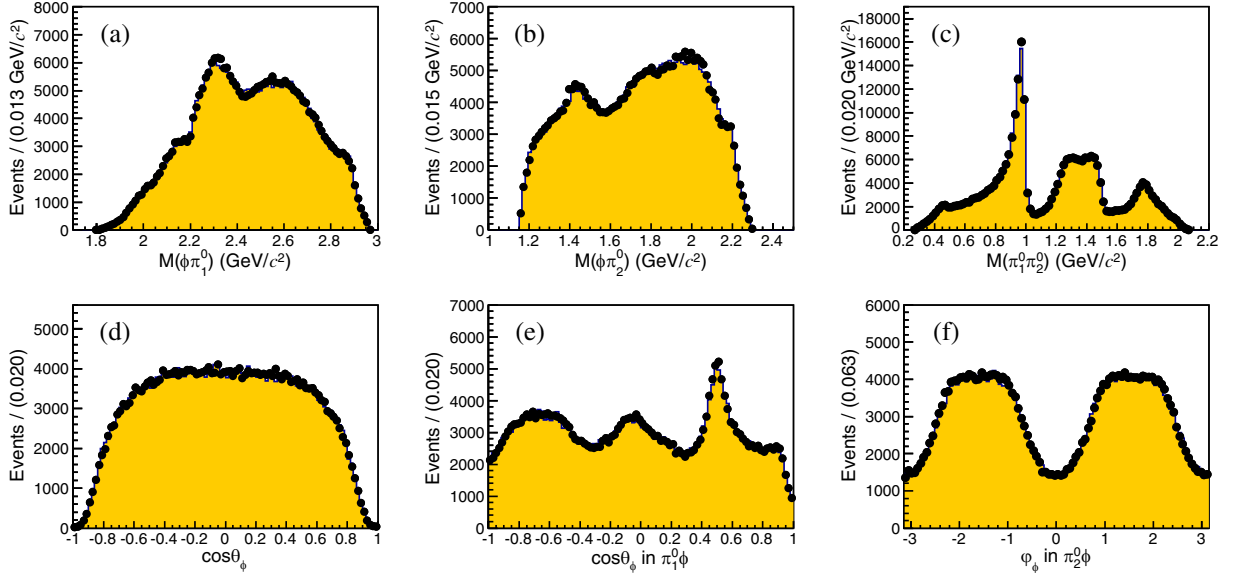


FIG. 5. Distributions of (a) $M(\phi\pi_1^0)$, (b) $M(\phi\pi_2^0)$, (c) $M(\pi_1^0\pi_2^0)$, (d) cosine of the polar angle of ϕ in the J/ψ rest frame, (e) cosine of the polar angle of ϕ in the $\pi_1^0\phi$ rest frame, and (f) azimuth of ϕ in the $\pi_2^0\phi$ rest frame of the $J/\psi \rightarrow \phi\pi^0\pi^0$ candidate events in data (dots with error bars are data) and the reweighted MC sample (orange shadowed regions).

tensor amplitudes [60]. Let A_R be the amplitude of a J/ψ decay process with the intermediate resonance R . For J/ψ radiative decays, the general form of A_R is written as

$$\begin{aligned}
 A_R(\vec{\xi}) &= \psi_\mu(p, m_\psi) e_\nu^*(q_1, m_\gamma) e_\alpha^*(q_2, m_\gamma) A_R^{\mu\nu\alpha}(\vec{\xi}) \\
 &= \psi_\mu(p, m_\psi) e_\nu^*(q_1, m_\gamma) e_\alpha^*(q_2, m_\gamma) \sum_i \Lambda_{R_i} U_{R_i}^{\mu\nu\alpha}(\vec{\xi}),
 \end{aligned}
 \tag{7}$$

where the sum runs over the number of independent amplitudes. The $\psi_\mu(p, m_\psi)$ is the polarization four-vector for J/ψ , and $e_\nu^*(q_i, m_\gamma)$ ($i = 1, 2$) are the polarization four-vectors for the two photons. m represents the spin projection, p and q are the four-momenta of J/ψ and photon; The Λ_{R_i} is the complex coupling coefficient of the amplitude; $U_{R_i}^{\mu\nu\alpha}(\vec{\xi})$ is the i th partial-wave amplitude for the intermediate resonance, it is constructed with the four-momenta

of the particles ($\vec{\xi}$) in the final state. Their specific expressions are given in Ref. [60].

In this analysis, the intermediate resonances decaying into $\gamma\phi$ (denoted as bc) are parametrized by a constant-width BW propagator,

$$f_{bc}^R = \frac{1}{M^2 - s_{bc} - i\frac{1}{c^2}M\Gamma}, \quad (8)$$

where M and Γ are the mass and width of the intermediate resonance R , respectively; s_{bc} is the invariant mass squared of $\gamma_i\phi$ system. The Breit-Wigner term for the nonresonant component is set to a constant in the partial-wave amplitude.

The complex coefficients of the amplitudes (relative magnitudes and phases) and the resonance parameters (masses and widths) are determined by an unbinned maximum likelihood fit to the data events. The likelihood is constructed following a method similar to the one used in Ref. [61].

The joint likelihood for observing N events in the data sample is then given by

$$\mathcal{L} = \prod_{i=1}^N \frac{|M(\vec{\xi}_i)|^2 \epsilon(\vec{\xi}_i) \Phi(\vec{\xi}_i)}{\sigma'}. \quad (9)$$

where $\epsilon(\vec{\xi})$ is the detection efficiency, $\Phi(\vec{\xi})$ is the standard element of PHSP, $M(\vec{\xi}) = \sum_R A_R(\vec{\xi})$ is the matrix element describing the decay $J/\psi \rightarrow \gamma\gamma\phi$, $A_R(\vec{\xi})$ is the amplitude corresponding to the intermediate resonance R , and $\sigma' \equiv \int |M(\vec{\xi})|^2 \epsilon(\vec{\xi}) \Phi(\vec{\xi}) d\vec{\xi}$ is the normalization integral.

Then the negative log-likelihood (NLL) value is represented by

$$-\ln \mathcal{L} = -\sum_{i=1}^N \ln |M(\vec{\xi}_i)|^2 + N \ln \sigma' - \sum_{i=1}^N \ln \epsilon(\vec{\xi}_i) \Phi(\vec{\xi}_i), \quad (10)$$

where the third term is a constant with no impact on the determination of the fit parameters and therefore is not considered in the fit.

The free parameters are optimized by MINUIT [62]. The normalization integral σ' is evaluated using MC simulation with importance sampling [63,64]. The MC sample of size N_{gen} is generated with signal events uniformly distributed in PHSP. These events are simulated by taking into account of detector response, and subjected to the same selection criteria of data, yielding a sample of N_{acc} accepted events. The normalization integral is computed as

$$\sigma' = \int |M(\vec{\xi})|^2 \epsilon(\vec{\xi}) \Phi(\vec{\xi}) d\vec{\xi} \propto \frac{1}{N_{\text{gen}}} \sum_j^{N_{\text{acc}}} |M(\vec{\xi}_j)|^2, \quad (11)$$

where the constant value of the PHSP integral $\int \Phi(\vec{\xi}) d\vec{\xi}$ is ignored.

Instead of modeling the background, the likelihood for the background is defined by the signal PDF [Eq. (9)]. The contribution to the negative log-likelihood from background events in the signal region is removed by subtracting the negative log-likelihood of events in the background samples. $\mathcal{L}_{\phi\pi^0\pi^0}$ and $\mathcal{L}_{\phi\pi^0(\phi\eta/\phi\eta')}$ denote the likelihoods of the $J/\psi \rightarrow \phi\pi^0\pi^0$ events and the remaining $J/\psi \rightarrow \phi\pi^0, \phi\eta, \phi\eta'$ events, respectively. Thus the fit minimizes the NLL given by

$$-\ln \mathcal{L}_{\text{sig}} = -(\ln \mathcal{L}_{\text{Qweighteddata}} - \ln \mathcal{L}_{\phi\pi^0\pi^0} - \omega_j \ln \cdot \mathcal{L}_{\phi\pi^0} - \omega_k \ln \cdot \mathcal{L}_{\phi\eta} - \omega_l \ln \cdot \mathcal{L}_{\phi\eta'}). \quad (12)$$

Here, $-\ln \mathcal{L}_{\text{sig}}$ represents the negative log-likelihood of signal events, with the normalization factors $\omega_j = 0.2$, $\omega_k = 2.0$, $\omega_l = 0.5$ for the $J/\psi \rightarrow \phi\pi^0, \phi\eta, \phi\eta'$ background events included. The $\mathcal{L}_{\text{Qweighteddata}}$ and $\mathcal{L}_{\phi\pi^0\pi^0}$ are calculated by

$$\mathcal{L}_{\text{Qweighteddata}} = \prod_{i=1}^N \frac{|M(\vec{\xi}_i)|^2 \epsilon(\vec{\xi}_i) \Phi(\vec{\xi}_i)}{\sigma'} \cdot Q_i, \quad (13)$$

$$\mathcal{L}_{\phi\pi^0\pi^0} = \prod_{m=1}^{N_{\phi\pi^0\pi^0}} \frac{|M(\vec{\xi}_m)|^2 \epsilon(\vec{\xi}_m) \Phi(\vec{\xi}_m)}{\sigma'} \cdot \mathcal{W}_m, \quad (14)$$

where Q_i represents the Q-factor for each event, and \mathcal{W}_m denotes the weight for the background events of $J/\psi \rightarrow \phi\pi^0\pi^0$. The $\mathcal{L}_{\phi\pi^0}$, $\mathcal{L}_{\phi\eta}$, and $\mathcal{L}_{\phi\eta'}$ are given as

$$\mathcal{L}_{\phi\pi^0(\phi\eta/\phi\eta')} = \prod_{i=1}^{N_{\phi\pi^0(\phi\eta/\phi\eta')}} \frac{|M(\vec{\xi}_i)|^2 \epsilon(\vec{\xi}_i) \Phi(\vec{\xi}_i)}{\sigma'}. \quad (15)$$

The log-likelihood is scaled by taking into account the statistical uncertainties of subtracted backgrounds [65].

The fitted event yield N_R of an intermediate resonance R is determined as

$$N_R = \frac{\sigma_R}{\sigma'} \cdot N_{\text{sig}}, \quad (16)$$

where N_{sig} the number of signal events after subtracting all backgrounds, and

$$\sigma_R = \frac{1}{N_{\text{gen}}} \sum_j^{N_{\text{acc}}} |A_R(\vec{\xi}_j)|^2 \quad (17)$$

is calculated with the same MC sample as the normalization integral σ' .

TABLE II. Pool of candidate resonances for the PWA.

0^{++}	0^{-+}	1^{++}	1^{-+}	2^{++}	2^{-+}
$f_0(1370)$	$\eta(1295)$	$f_1(1285)$	$\eta_1(1855)$	$f_2(1270)$	$\eta_2(1645)$
$f_0(1500)$	$\eta(1405)$	$f_1(1420)$		$f_2(1430)$	$\eta_2(1870)$
$f_0(1710)$	$\eta(1475)$	$f_1(1510)$		$f_2(1525)$	
$f_0(2020)$	$\eta(1760)$			$f_2(1565)$	
$f_0(2100)$	$X(1835)$			$f_2(1640)$	
$f_0(2200)$	$\eta(2225)$			$f_2(1810)$	
$f_0(2330)$	$X(2370)$			$f_2(1910)$	
	η_c			$f_2(1950)$	
				$f_2(2010)$	
				$f_2(2150)$	
				$f_J(2220)$	
				$f_2(2300)$	
				$f_2(2340)$	

The interference cross section between two different resonances is calculated by

$$\sigma_{R_1, R_2} = \frac{1}{N_{\text{acc}}} \sum_k \sum_{j_1}^{N_{W_1}} \sum_{j_2}^{N_{W_2}} \left((A_{j_1})_k (A_{j_2}^*)_k + (A_{j_1}^*)_k (A_{j_2})_k \right), \quad (18)$$

where N_{W_1} and N_{W_2} are the numbers of the independent partial-wave amplitudes of R_1 and R_2 , respectively.

The detection efficiency ϵ_R of the intermediate resonance R is obtained by the partial-wave amplitude weighted MC sample,

$$\epsilon_R = \frac{\sum_j^{N_{\text{acc}}} |A_R(\vec{\xi}_j)|^2}{\sum_n^{N_{\text{gen}}} |A_R(\vec{\xi}_n)|^2}. \quad (19)$$

Finally, the BF of $J/\psi \rightarrow \gamma R$, $R \rightarrow \gamma \phi$ is calculated by

$$\mathcal{B}(J/\psi \rightarrow \gamma R \rightarrow \gamma \phi) = \frac{N_R}{N_{J/\psi} \cdot \epsilon_R \cdot \mathcal{B}(\phi \rightarrow K^+ K^-)}, \quad (20)$$

where $N_{J/\psi}$ is the total number of J/ψ event, which is $(10087 \pm 44) \times 10^{-6}$; ϵ_R is the detection efficiency of the resonance R ; $\mathcal{B}(\phi \rightarrow K^+ K^-) = (49.1 \pm 0.5)\%$ is the BF of $\phi \rightarrow K^+ K^-$ taken from the PDG [4].

VI. ANALYSIS RESULTS

In this analysis, we consider all kinematically allowed resonances with $J^{PC} = 0^{++}, 0^{-+}, 1^{++}, 1^{-+}, 2^{++}$, and 2^{-+} as listed from the PDG [4]. Additionally, we take into account an exotic structure $\eta_1(1855)$ recently observed in $J/\psi \rightarrow \gamma \eta \eta'$ by BESIII [29,38] and a glueball candidate $X(2370)$ observed in $J/\psi \rightarrow \gamma \pi^+ \pi^- \eta'$ [18]. We also consider nonresonant contributions with certain $J^{PC} = 0^{++}, 0^{-+}, 1^{++}, 1^{-+}, 2^{++}$ for the $\gamma \phi$ system. All possible resonances listed in Table II are taken into account, and their statistical significances are evaluated. Only the components with statistical significance greater than 5σ are kept in the baseline solution. The statistical significance of each resonance is determined from the relative changes of optimal NLL values when including and excluding it in the fit, assuming the χ^2 distribution hypothesis and taking into account the change in the number of degrees of freedom.

Due to limited statistics, the masses, widths and J^{PC} of all candidate states are fixed to individual PDG values. However, for $\eta(1405)$ and $X(1835)$, their masses and widths are free. Changing the J^{PC} in the baseline set of amplitudes to other hypotheses results in a worse negative log-likelihood by at least 13.2 units. The results of the

TABLE III. The masses and widths of resonances, significance and the product BFs $\mathcal{B}(J/\psi \rightarrow \gamma R \rightarrow \gamma \phi)$ of each component in the PWA fit using the baseline set of amplitudes. The first uncertainties are statistical and the second are systematic. The masses and widths of the f -states and η_c are fixed to the PDG values [4].

Resonance	M (MeV/ c^2)	Γ (MeV)	$\mathcal{B}(\times 10^{-6})$	Significance
$f_1(1285)$	1281.9	22.7	$0.29 \pm 0.03^{+0.11}_{-0.09}$	17.3σ
$f_1(1420)$	1426.3	54.5	$0.55 \pm 0.07^{+0.18}_{-0.17}$	9.0σ
$\eta(1405)$	$1422.0 \pm 2.1^{+5.9}_{-7.8}$	$86.3 \pm 2.7^{+6.6}_{-17.4}$	$3.57 \pm 0.18^{+0.59}_{-0.61}$	18.9σ
$f_1(1510)$	1518.0	73.0	$0.78 \pm 0.09^{+0.34}_{-0.30}$	5.3σ
$f_2(1525)$	1517.4	86.0	$2.76 \pm 0.18^{+0.90}_{-0.61}$	16.4σ
$X(1835)$	$1849.3 \pm 3.0^{+7.6}_{-10.0}$	$179.6 \pm 8.7^{+22.5}_{-27.9}$	$3.37 \pm 0.19^{+0.78}_{-1.10}$	15.3σ
$f_2(1950)$	1936.0	464.0	$9.96 \pm 0.60^{+3.44}_{-2.13}$	13.1σ
$f_2(2010)$	2011.0	202.0	$4.63 \pm 0.43^{+1.42}_{-1.46}$	11.3σ
$f_0(2200)$	2187.0	207.0	$0.20 \pm 0.04^{+0.05}_{-0.07}$	6.3σ
η_c	2983.9	32.0	$0.21 \pm 0.03^{+0.05}_{-0.07}$	12.9σ

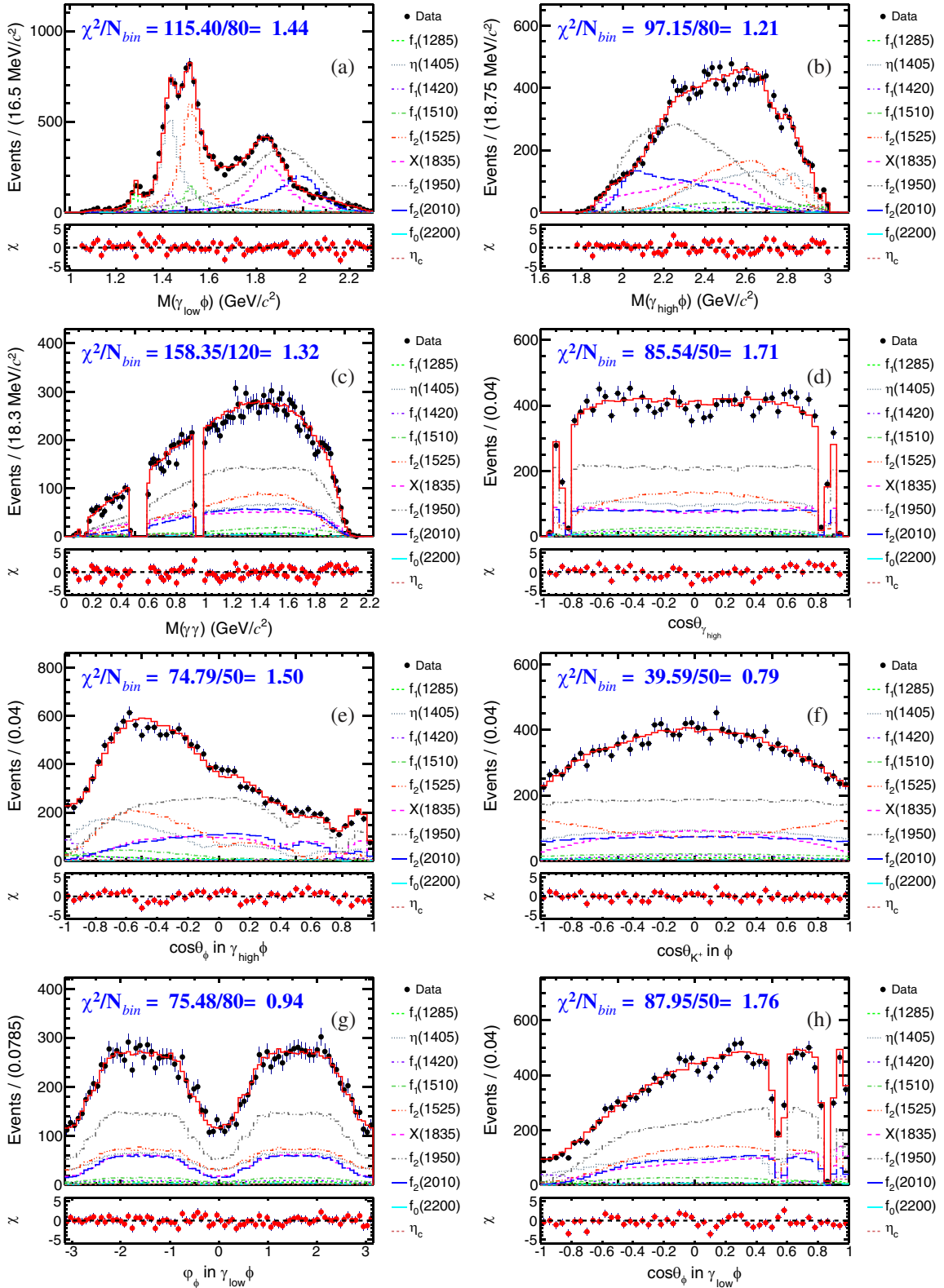


FIG. 6. PWA fit projections on (a) $M(\gamma_{\text{low}}\phi)$, (b) $M(\gamma_{\text{high}}\phi)$, (c) $M(\gamma\gamma)$, (d) cosine of polar angle of the high-energy photon in the rest frame of J/ψ , (e) cosine of polar angle of ϕ in the rest frame of $\gamma_{\text{high}}\phi$, (f) cosine of polar angle of K^+ in the rest frame of ϕ , (g) azimuth of ϕ in the rest frame of $\gamma_{\text{low}}\phi$, and (h) cosine of polar angle of ϕ in the rest frame of $\gamma_{\text{low}}\phi$. The black dots with error bars represent data, the red lines represent the projections of PWA fit, and the bashed lines represent contributions of each component in the baseline solution.

TABLE IV. Fit fractions (σ_R/σ') of each component and interference fractions ($\sigma_{R_1,R_2}/\sigma'$) between two components in the baseline solution. The uncertainties are statistical only. All the values are given in %.

Resonance	$f_1(1285)$	$f_1(1420)$	$\eta(1405)$	$f_1(1510)$	$f_2(1525)$	$X(1835)$	$f_2(1950)$	$f_2(2010)$	$f_0(2200)$	η_c
$f_1(1285)$	1.84 ± 0.16	0.54 ± 0.11	0.34 ± 0.08	-0.26 ± 0.11	-0.31 ± 0.04	-0.34 ± 0.09	-0.14 ± 0.07	-0.09 ± 0.05	0.00 ± 0.00	0.07 ± 0.03
$f_1(1420)$	3.94 ± 0.42	3.94 ± 0.42	-0.30 ± 0.21	-2.38 ± 0.45	-0.16 ± 0.22	1.00 ± 0.18	-3.42 ± 0.32	2.45 ± 0.22	0.00 ± 0.00	-0.18 ± 0.05
$\eta(1405)$			21.85 ± 0.79	-0.78 ± 0.17	-0.29 ± 0.09	2.14 ± 0.82	-0.19 ± 0.09	-0.14 ± 0.05	0.02 ± 0.01	1.66 ± 0.16
$f_1(1510)$				5.62 ± 0.56	0.55 ± 0.42	0.17 ± 0.16	4.85 ± 0.45	-3.10 ± 0.27	-0.13 ± 0.05	-0.13 ± 0.05
$f_2(1525)$					18.74 ± 0.95	0.09 ± 0.06	7.83 ± 0.96	-2.14 ± 0.45	0.18 ± 0.06	-0.12 ± 0.01
$X(1835)$						19.03 ± 0.76	1.88 ± 0.17	-1.12 ± 10.13	0.00 ± 0.00	-2.13 ± 0.14
$f_2(1950)$							60.94 ± 2.78	-72.11 ± 4.56	-1.06 ± 0.21	0.24 ± 0.04
$f_2(2010)$								19.03 ± 0.76	1.85 ± 0.26	-0.14 ± 0.02
$f_0(2200)$									30.78 ± 2.45	0.01 ± 0.00
η_c										1.28 ± 0.14

baseline fit including the masses, widths and product BFs are listed in Table III. The baseline results show that the structure in the vicinity of $1.4 \text{ GeV}/c^2$, as shown in Fig. 6(a), needs to be described by $\eta(1405)$ and $f_1(1420)$ in the $\gamma\phi$ system. The measured mass and width of $\eta(1405)$ are $(1422.0 \pm 2.1^{+5.9}_{-7.8}) \text{ MeV}/c^2$ and $(86.3 \pm 2.7^{+6.6}_{-17.4}) \text{ MeV}$, respectively. The spin-parity of the structure with mass around $1.8 \text{ GeV}/c^2$ is determined to be 0^{-+} . Its mass and width are measured to be $(1849.3 \pm 3.0^{+7.6}_{-10.0}) \text{ MeV}/c^2$ and $(179.6 \pm 8.7^{+22.5}_{-27.9}) \text{ MeV}$, which are consistent with those of the $X(1835)$ measured in $J/\psi \rightarrow \gamma K_S^0 K_S^0 \eta$ [11]. The fit fractions of each component (defined as σ_R/σ') and their interference fractions (defined as $\sigma_{R_1,R_2}/\sigma'$) are shown in Table IV. The comparisons between the data and the PWA fit projections for the distributions of $M(\gamma_{\text{low}}\phi)$, $M(\gamma_{\text{high}}\phi)$, $M(\gamma\gamma)$ and several angular distributions are shown in Fig. 6. The χ^2/N_{bin} is displayed on each figure to demonstrate the goodness of fit, where N_{bin} is the number of bins in each histogram, and χ^2 is defined as

$$\chi^2 = \sum_{i=1}^{N_{\text{bin}}} \frac{(n_i - \nu_i)^2}{\nu_i}, \quad (21)$$

where n_i and ν_i are the numbers of events of the data and the fit projections with the baseline set of amplitudes in the i th bin of each figure, respectively.

All other possible resonances have a statistical significance less than 5σ when added to the baseline set of amplitudes with fixed resonance parameters as listed in Table III. In addition, the statistical significances of all possible nonresonant contributions are also less than 5σ , as shown in Table V. Among them, the $f_0(2020)$ has a significance of 4.9σ , but with a fit fraction much less than 1%. In the following text, the upper limit on the BF of $J/\psi \rightarrow \gamma f_0(2020) \rightarrow \gamma\gamma\phi$ is presented at 90% confidence level. The impact of the inclusion of $f_0(2020)$ on the PWA result is assigned as a systematic uncertainty, as discussed in Sec. VI. To investigate additional possible contributions, resonances with different J^{PC} (0^{++} , 0^{-+} , 1^{++} , 1^{-+} , 2^{++} , 2^{-+}) and different masses and widths are added to the baseline set of amplitudes. No significant contribution is found.

A further check on the pseudoscalar structure with mass around $1.4 \text{ GeV}/c^2$ is performed. If the mass and width of the pseudoscalar state are fixed to the PDG values of $\eta(1405)$ or $\eta(1475)$ [4], the log-likelihood worsens by 45.6 or 56.2. Another test includes an additional $\eta(1475)$ with parameters fixed at the PDG values or free resonance parameters in the baseline model, the statistical significances of these contributions are 2.3σ and 3.9σ . These results indicate that the possibility of a second η state around $1.4 \text{ GeV}/c^2$ is not excluded.

TABLE V. Changes in the negative log-likelihood ($\Delta \ln \mathcal{L}$) and in the number of degrees of freedom ($\Delta d.o.f.$) by considering additional resonances and the corresponding statistical significance. The $\Delta d.o.f.$ is determined by the complex coefficient of independent partial wave [60].

Resonance	$\Delta \ln \mathcal{L}$	$\Delta d.o.f.$	Significance
$f_2(1270)$	3.9	18	0.1σ
$\eta(1295)$	0.1	2	0.1σ
$f_0(1370)$	1.4	2	1.2σ
$f_0(1430)$	1.4	2	1.2σ
$f_2(1430)$	4.9	18	0.1σ
$\eta(1475)$	8.6	2	3.7σ
$f_0(1500)$	0.8	2	0.7σ
$f_2(1565)$	12.4	18	1.5σ
$f_2(1640)$	7.4	18	0.4σ
$\eta_2(1645)$	3.3	18	0.0σ
$f_0(1710)$	2.7	2	1.8σ
$\eta(1760)$	0.6	2	0.6σ
$f_2(1810)$	10.3	18	1.0σ
$\eta_1(1855)$	2.9	8	0.4σ
$\eta_2(1870)$	11.6	18	1.3σ
$f_2(1910)$	9.6	18	0.9σ
$f_0(2020)$	13.6	2	4.9σ
$f_0(2100)$	7.4	2	3.4σ
$f_2(2150)$	9.6	18	0.9σ
$f_J(2220)$	13.7	18	1.8σ
$\eta(2225)$	0.6	2	0.6σ
$f_2(2300)$	16.8	18	2.5σ
$f_0(2330)$	12.0	2	4.5σ
$f_2(2340)$	15.2	18	2.1σ
$X(2370)$	0.4	2	0.4σ
0^{++} PHSP	0.9	2	0.9σ
0^{-+} PHSP	4.1	2	2.4σ
1^{++} PHSP	5.9	8	1.5σ
2^{++} PHSP	18.4	18	2.8σ
2^{-+} PHSP	5.9	18	0.2σ

The PWA result shows that there is no evidence for the $\eta(1295)$, $\eta(1475)$, $\eta_1(1855)$, $f_0(2020)$ and $X(2370)$ in the $\gamma\phi$ system. The same approach as in Ref. [66] is used to determine the upper limits of the production of these five states. The systematic uncertainties of these upper limits are calculated with same method as for the baseline solution, cf. Sec. VII, and are summed in quadrature with the statistical uncertainty for each respective yield. The resulting uncertainty is used to determine the 90% confidence level deviation, and added to the updated nominal yield of the candidate state to obtain the corresponding upper limit on the BF. As a result, the upper limits are determined to be $\mathcal{B}(J/\psi \rightarrow \gamma\eta(1295) \rightarrow \gamma\gamma\phi) < 8.37 \times 10^{-7}$, $\mathcal{B}(J/\psi \rightarrow \gamma\eta(1475) \rightarrow \gamma\gamma\phi) < 3.80 \times 10^{-7}$, $\mathcal{B}(J/\psi \rightarrow \gamma\eta_1(1855) \rightarrow \gamma\gamma\phi) < 4.74 \times 10^{-6}$, $\mathcal{B}(J/\psi \rightarrow \gamma f_0(2020) \rightarrow \gamma\gamma\phi) < 2.41 \times 10^{-6}$ and $\mathcal{B}(J/\psi \rightarrow \gamma X(2370) \rightarrow \gamma\gamma\phi) < 1.08 \times 10^{-7}$.

VII. SYSTEMATIC UNCERTAINTIES

A. Systematic uncertainties due to event selection

The systematic uncertainties that arise from event selection impact the BF measurements. The sources contributing to the uncertainty are listed below.

- (i) Total number of J/ψ events. The uncertainty due to the total number of J/ψ events is 0.4% according to Ref. [43].
- (ii) Kaon tracking and PID. The charged kaon tracking and PID efficiencies are studied using control sample $J/\psi \rightarrow K_S^0 K^\pm \pi^\mp$, $K_S^0 \rightarrow \pi^+ \pi^-$ [67]. The systematic uncertainty from tracking and PID is estimated to be 1% per kaon.
- (iii) Photon detection. The photon detection efficiency is studied using $J/\psi \rightarrow \rho\pi^0 \rightarrow \pi^+ \pi^- \pi^0$ [68] control sample. The systematic uncertainty of photon detection is assigned to be 1% per photon.
- (iv) Kinematic fit. The track helix parameter correction method [69] is used to investigate the systematic uncertainty associated with the 4C kinematic fit. The difference in the detection efficiencies with and without the helix parameter correction, 1.2%, is taken as the systematic uncertainty.

The total systematic uncertainty from event selection is determined to be 3.5%, obtained as a quadratic sum of the contributions discussed above.

B. Systematic uncertainties due to PWA

Systematic uncertainty from the PWA impacts both BFs and resonance parameters. The sources of this uncertainty are described below.

- (i) Mass window cuts: The uncertainties from mass window requirements of π^0 , η , η' are estimated by enlarging or shrinking each mass window within 2 MeV/ c^2 . The largest changes in the measured masses and widths of $\eta(1405)$, $X(1835)$ and the BFs are assigned as the systematic uncertainties.
- (ii) Non- ϕ backgrounds: The uncertainty due to the Q -factor method [56] is obtained by smearing the nominal Q -value in each event by a Gaussian distribution with standard deviation

$$\sigma_Q^2 = \sum_{ij} \frac{\partial Q}{\partial \alpha_i} (C_\alpha^{-1})_{ij} \frac{\partial Q}{\partial \alpha_j}, \quad (22)$$

where Q is the Q -factor, α_i are the measurable quantities and C_α is the full covariance matrix. The new Q -factors are used in the PWA, and the differences between the nominal and new fits are assigned as the systematic uncertainties.

- (iii) ϕ backgrounds: The ‘‘datalike’’ MC distributions of $J/\psi \rightarrow \phi\pi^0\pi^0$ have been obtained using a machine learning-based multidimensional reweighting method [58]. The systematic uncertainties are

TABLE VI. Systematic uncertainties on the masses and widths of $\eta(1405)$ and $X(1835)$.

Source	$\eta(1405)$		$X(1835)$	
	ΔM (MeV/ c^2)	$\Delta\Gamma$ (MeV)	ΔM (MeV/ c^2)	$\Delta\Gamma$ (MeV)
π^0 mass window cut	2.5	2.7	3.1	9.4
η mass window cut	2.0	3.0	1.0	8.8
η' mass window cut	1.6	1.9	0.5	2.6
Q -factor method	2.0	1.9	0.4	9.4
Multidimensional reweighting method	2.5	2.7	3.1	8.9
Resonance parameters	2.0	2.7	3.0	8.6
Extra resonances	+2.8 -5.8	+2.2 -16.3	+5.4 -8.4	+9.7 -19.1
Total	+5.9 -7.8	+6.6 -17.4	+7.7 -10.0	+22.5 -27.9

estimated by changing the kinematic variables utilized for machine learning training. The kinematic variables are changed from four-momenta of π_1^0 , π_2^0 and ϕ , $M(\phi\pi_1^0)$, $M(\phi\pi_2^0)$, $M(\pi_1^0\pi_2^0)$, $\cos\theta_\phi$, $\cos\theta_{\pi_1^0}$, and $\cos\theta_{\pi_2^0}$ to $P_z(\pi_1^0)$, $E(\pi_1^0)$, $P_z(\pi_2^0)$, $E(\pi_2^0)$, $P_z(\phi)$, $E(\phi)$, $M(\phi\pi_1^0)$, $M(\phi\pi_2^0)$, $M(\pi_1^0\pi_2^0)$, φ_ϕ , $\varphi_{\pi_1^0}$, and $\varphi_{\pi_2^0}$. The changes in the results are regarded as the systematic uncertainties. Since the remaining contributions of $J/\psi \rightarrow \phi\pi^0$, $J/\psi \rightarrow \phi\eta$, and $J/\psi \rightarrow \phi\eta'$ are small ($\sim 0.8\%$), their impact on the PWA results is negligible.

- (iv) Resonance parameters: In the baseline solution, the resonance parameters of $f_1(1285)$, $f_1(1420)$, $f_2(2010)$, $f_0(2200)$, $f_1(1510)$, $f_2(1950)$, $f_2(1525)$, and η_c are fixed to the PDG [4] values. Alternative fits are performed with these resonance parameters varied within one standard deviation of individual PDG value. The changes in the results are taken as the corresponding systematic uncertainties.
- (v) Additional resonances: The uncertainties arising from possible additional resonances are estimated by adding the $f_0(2020)$, $\eta(1405)$, 1^{++} PHSP, 2^{++} PHSP, or $\eta_2(1870)$ into the baseline fit individually. These candidate resonances are the most significant additional resonances for each possible J^{PC} . The

resulting changes in the measurements are assigned as the systematic uncertainties.

For each measurement, the individual uncertainties are assumed to be independent and are added in quadrature to obtain the total systematic uncertainty. The sources of systematic uncertainties in the measurements of masses and widths of $\eta(1405)$ and $X(1835)$ are summarized in Table VI. The relative systematic uncertainties of the BF measurements are summarized in Table VII.

VIII. SUMMARY

To investigate the structures in the $\gamma\phi$ system of $J/\psi \rightarrow \gamma\gamma\phi$ [42], a PWA of this decay is performed for the first time, by using a sample of $(10087 \pm 44) \times 10^6$ J/ψ events collected with the BESIII detector. The PWA result shows that the $J/\psi \rightarrow \gamma R$, $R \rightarrow \gamma\phi$ process has predominantly 2^{++} components. The decays of $\eta(1405)$, $X(1835)$, several f -states, and η_c into $\gamma\phi$ are observed with statistical significance greater than 5σ . The f -states are associated with $f_1(1285)$, $f_1(1420)$, $f_1(1510)$, $f_2(1525)$, $f_2(1950)$, $f_2(2010)$, and $f_0(2200)$. The decays of $f_1(1285)$, $f_1(1420)$, $\eta(1405)$, and $X(1835)$ to the $\gamma\phi$ final state have been confirmed, while the decays of the other resonances to the $\gamma\phi$ final state have been observed for the first time.

TABLE VII. Relative systematic uncertainties on $\mathcal{B}(J/\psi \rightarrow \gamma R \rightarrow \gamma\gamma\phi)(\%)$.

Source	$f_1(1285)$	$f_1(1420)$	$f_0(2200)$	$f_2(2010)$	$\eta(2983)$	$\eta(1405)$	$f_1(1510)$	$X(1835)$	$f_2(1950)$	$f_2(1525)$
Event selection	3.5	3.5	3.5	3.5	3.5	3.5	3.5	3.5	3.5	3.5
π^0 mass window cut	10.7	6.6	6.3	13.7	11.8	6.2	8.5	12.1	9.2	7.1
η mass window cut	7.1	5.2	5.3	19.8	9.6	6.1	12.1	8.5	3.1	3.6
η' mass window cut	13.7	11.3	9.3	7.1	11.8	0.3	19.8	9.1	8.5	4.7
Q -factor method	12.7	14.1	6.6	4.7	6.8	1.9	17.7	8.8	1.4	7.2
Multidimensional reweighting method	15.2	13.8	6.5	6.6	9.3	0.9	7.7	3.9	4.8	11.2
Resonance parameters	12.2	6.5	4.7	6.5	0.9	7.1	15.0	0.5	15.2	11.3
Extra resonances	+23.7 -3.4	+20.7 -17.1	+17.8 -28.5	+13.7 -15.7	+0.0 -24.7	+12.4 -11.7	+25.3 -17.0	+11.7 -26.8	+27.6 -4.9	+25.9 -3.2
Total	+38.3 -30.3	+32.7 -30.6	+24.3 -33.0	+30.6 -31.6	+22.7 -33.6	+17.2 -16.7	+43.1 -38.9	+23.3 -33.5	+34.6 -21.4	+32.8 -20.3

In the $\gamma\phi$ system, only one pseudoscalar particle, $\eta(1405)$, is identified with a mass around $1.4 \text{ GeV}/c^2$. The measured product BF of $\eta(1405)$ is $\mathcal{B}(J/\psi \rightarrow \gamma\eta(1405) \rightarrow \gamma\gamma\phi) = (3.57 \pm 0.18_{-0.61}^{+0.59}) \times 10^{-6}$. Due to the lack of direct coupling between glueballs and photons, the glueball decay into $\gamma\phi$ is suppressed. The $\eta(1405)$ observed in $J/\psi \rightarrow \gamma\gamma\phi$ is unfavorable to be a glueball, making it more likely to be an excited state of η' . Furthermore, the significance of an additional $\eta(1475)$ is evaluated to be 3.7σ , indicating that the presence of the $\eta(1475)$ cannot be excluded.

The J^{PC} of $X(1835)$ is confirmed to be 0^{-+} . The mass, width and product of BF of $X(1835)$ are determined to be $(1849.3 \pm 3.0_{-10.0}^{+7.6}) \text{ MeV}/c^2$, $(179.6 \pm 8.7_{-27.9}^{+22.5}) \text{ MeV}$ and $\mathcal{B}(J/\psi \rightarrow \gamma X(1835) \rightarrow \gamma\gamma\phi) = (3.37 \pm 0.19_{-1.10}^{+0.78}) \times 10^{-6}$, respectively. The observation of the decay $X(1835) \rightarrow \gamma\phi$ indicates that the $X(1835)$ is a second radial excited state of η' containing $s\bar{s}$ quarks [14,15].

Observation of the $\eta_c \rightarrow \gamma\phi$ decay, which is the first observation of the radiative decay of η_c , is important for studying the properties of charmonium, such as the decays of J/ψ and χ_{cJ} [70,71].

The decays of $f_1(1510)$, $f_2(1525)$, $f_2(1950)$, $f_2(2010)$ and $f_0(2200)$ to $\gamma\phi$ are observed for the first time. Accurate measurement of the $R \rightarrow \gamma\phi$ decay provides crucial theoretical input for understanding the properties of these particles [28,40,72].

No evidence of $\eta(1295)$, $\eta_1(1855)$ or $X(2370)$ is observed in the process of $J/\psi \rightarrow \gamma\gamma\phi$. The possible existence of $\eta(1295)$ cannot be excluded yet, because the production rate of $\eta(1295)$ in J/ψ radiative decays is predicted to be suppressed due to SU(3) flavor symmetry [73]. The measured upper limit on the product BF of $J/\psi \rightarrow \gamma X(2370) \rightarrow \gamma\gamma\phi$ and $\mathcal{B}(J/\psi \rightarrow \gamma\eta_1(1855) \rightarrow \gamma\gamma\phi)$ does not contradict the theoretical expectations for the proposed natures, pseudoscalar glueball for $X(2370)$ and hybrid state for $\eta_1(1855)$, as discussed in the introduction. A larger sample of J/ψ in the future will be helpful to pin down the properties of these states.

ACKNOWLEDGMENTS

The BESIII Collaboration thanks the staff of BEPCII and the IHEP computing center for their strong support. This work is supported in part by National Key R&D Program of China under Contracts No. 2020YFA0406300,

No. 2020YFA0406400; National Natural Science Foundation of China (NSFC) under Contracts No. 11635010, No. 11735014, No. 11835012, No. 11922511, No. 11935015, No. 11935016, No. 11935018, No. 11961141012, No. 12022510, No. 12025502, No. 12035009, No. 12035013, No. 12061131003, No. 12192260, No. 12192261, No. 12192262, No. 12192263, No. 12192264, No. 12192265, No. 12221005, No. 12225509, No. 12235017, No. 12361141819; the Chinese Academy of Sciences (CAS) Large-Scale Scientific Facility Program; the CAS Center for Excellence in Particle Physics (CCEPP); Joint Large-Scale Scientific Facility Funds of the NSFC and CAS under Contract No. U1832207; CAS Key Research Program of Frontier Sciences under Contracts No. QYZDJ-SSW-SLH003, No. QYZDJ-SSW-SLH040; CAS Project for Young Scientists in Basic Research YSBR-101; 100 Talents Program of CAS; The Institute of Nuclear and Particle Physics (INPAC) and Shanghai Key Laboratory for Particle Physics and Cosmology; ERC under Contract No. 758462; European Union's Horizon 2020 research and innovation programme under Marie Skłodowska-Curie grant agreement under Contract No. 894790; German Research Foundation DFG under Contracts No. 443159800, No. 455635585, Collaborative Research Center No. CRC 1044, No. FOR5327, No. GRK 2149; Istituto Nazionale di Fisica Nucleare, Italy; Ministry of Development of Turkey under Contract No. DPT2006K-120470; National Research Foundation of Korea under Contract No. NRF-2022R1A2C1092335; National Science and Technology fund of Mongolia; National Science Research and Innovation Fund (NSRF) via the Program Management Unit for Human Resources & Institutional Development, Research and Innovation of Thailand under Contract No. B16F640076; Polish National Science Centre under Contract No. 2019/35/O/ST2/02907; The Swedish Research Council; U.S. Department of Energy under Contract No. DE-FG02-05ER41374.

DATA AVAILABILITY

The data that support the findings of this article are not publicly available because they are owned by a third party and the terms of use prevent public distribution. The data are available from the authors upon reasonable request.

- [1] E. Klempt and A. Zaitsev, *Phys. Rep.* **454**, 1 (2007).
- [2] A. Benhamida and L. Semlala, [arXiv:2206.09026](https://arxiv.org/abs/2206.09026).
- [3] H. X. Chen, W. Chen, X. Liu, Y. R. Liu, and S. L. Zhu, *Rep. Prog. Phys.* **86**, 026201 (2023).
- [4] R. L. Workman *et al.* (Particle Data Group), *Prog. Theor. Exp. Phys.* **2022**, 083C01 (2022).
- [5] A. Lanaro, *Nucl. Phys. B, Proc. Suppl.* **56**, 123 (1997).
- [6] M. Ablikim *et al.* (BES Collaboration), *Chin. Phys. C* **44**, 040001 (2020).
- [7] G. S. Bali, K. Schilling, A. Hulsebos, A. C. Irving, C. Michael, and P. W. Stephenson (UKQCD Collaboration), *Phys. Lett. B* **309**, 378 (1993).
- [8] Y. Chen *et al.*, *Phys. Rev. D* **73**, 014516 (2006).
- [9] A. Lanaro, *Nucl. Phys. B, Proc. Suppl.* **136**, 56 (1997).
- [10] M. Ablikim *et al.* (BES Collaboration), *Phys. Rev. Lett.* **95**, 262001 (2005).
- [11] M. Ablikim *et al.* (BESIII Collaboration), *Phys. Rev. Lett.* **115**, 091803 (2015).
- [12] B. Loiseau and S. Wycech, *Phys. Rev. C* **72**, 011001 (2005).
- [13] G. J. Ding and M. L. Yan, *Eur. Phys. J. A* **28**, 351 (2006).
- [14] J. S. Yu, Z. F. Sun, X. Liu, and Q. Zhao, *Phys. Rev. D* **83**, 114007 (2011).
- [15] T. Huang and S. L. Zhu, *Phys. Rev. D* **73**, 014023 (2006).
- [16] N. Kochelev and D. P. Min, *Phys. Rev. D* **72**, 097520 (2005).
- [17] M. Ablikim *et al.* (BESIII Collaboration), *Phys. Rev. Lett.* **106**, 072002 (2011).
- [18] M. Ablikim *et al.* (BESIII Collaboration), *Phys. Rev. Lett.* **129**, 042001 (2022).
- [19] M. Ablikim *et al.* (BESIII Collaboration), *Phys. Rev. Lett.* **132**, 181901 (2024).
- [20] C. Deng, J. Ping, Y. Yang, and F. Wan, *Phys. Rev. D* **86**, 014008 (2012).
- [21] B. D. Wan, S. Q. Zhang, and C. F. Qiao, *Phys. Rev. D* **105**, 014016 (2022).
- [22] L. M. Wang, Q. S. Zhou, C. Q. Pang, and X. Li, *Phys. Rev. D* **102**, 114034 (2020).
- [23] N. Su and H. X. Che, *Phys. Rev. D* **106**, 014023 (2022).
- [24] L. C. Gui, J. M. Dong, Y. Chen, and Y. B. Yang, *Phys. Rev. D* **100**, 054511 (2019).
- [25] J. F. Liu, G. J. Ding, and M. L. Yan, *Phys. Rev. D* **82**, 074026 (2010).
- [26] W. I. Eshraim, S. Janowski, F. Giacosa, and D. H. Rischke, *Phys. Rev. D* **87**, 054036 (2013).
- [27] R. Zhang, W. Sun, Y. Chen, M. Gong, L. C. Gui, and Z. Liu, *Phys. Lett. B* **827**, 136960 (2022).
- [28] F. Hechenberger, J. Leutgeb, and A. Rebhan, *Phys. Rev. D* **107**, 114020 (2023).
- [29] M. Ablikim *et al.* (BESIII Collaboration), *Phys. Rev. D* **105**, 072002 (2022).
- [30] H. X. Chen, N. Su, and S. L. Zhu, *Chin. Phys. Lett.* **39**, 051201 (2022).
- [31] L. Qiu and Q. Zhao, *Chin. Phys. C* **46**, 051001 (2022).
- [32] V. Shastry, C. S. Fischer, and F. Giacosa, *Phys. Lett. B* **834**, 137478 (2022).
- [33] X. K. Dong, Y. H. Lin, and B. S. Zou, *Sci. China Phys. Mech. Astron.* **65**, 261011 (2022).
- [34] F. Yang, H. Q. Zhu, and Y. Huang, *Nucl. Phys.* **A1030**, 122571 (2023).
- [35] H. X. Chen, A. Hosaka, and S. L. Zhu, *Phys. Rev. D* **78**, 117502 (2008).
- [36] B. D. Wan, S. Q. Zhang, and C. F. Qiao, *Phys. Rev. D* **106**, 074003 (2022).
- [37] B. Chen, S. Q. Luo, and X. Liu, *Phys. Rev. D* **108**, 054034 (2023).
- [38] Y. Huang and H. Q. Zhu, *J. Phys. G* **50**, 095002 (2023).
- [39] F. Y. Chen, X. Y. Jiang, Y. Chen, M. Gong, Z. F. Liu, C. J. Shi, and W. Sun, *Phys. Rev. D* **107**, 054511 (2023).
- [40] F. E. Close, A. Donnachie, and Yu. S. Kalashnikova, *Phys. Rev. D* **67**, 074031 (2003).
- [41] V. Crede and C. A. Meyer, *AIP Conf. Proc.* **1182**, 471 (2009).
- [42] M. Ablikim *et al.* (BESIII Collaboration), *Phys. Rev. D* **97**, 051101 (2018).
- [43] M. Ablikim *et al.* (BESIII Collaboration), *Chin. Phys. C* **46**, 074001 (2022).
- [44] M. Ablikim *et al.* (BESIII Collaboration), *Nucl. Instrum. Methods Phys. Res., Sect. A* **614**, 345 (2010).
- [45] C. H. Yu *et al.*, *Proceedings of IPAC2016, Busan, Korea* (2016), <https://accelconf.web.cern.ch/ipac2016/doi/JACoW-IPAC2016-TUYA01.html>.
- [46] J. Lu, Y. Xiao, and X. Ji, *Radiat. Detect. Technol. Methods* **4**, 337 (2020).
- [47] J. W. Zhang, L. H. Wu, S. S. Sun *et al.*, *Radiat. Detect. Technol. Methods* **6**, 289 (2022).
- [48] X. Li *et al.*, *Radiat. Detect. Technol. Methods* **1**, 13 (2017); Y. X. Guo *et al.*, *Radiat. Detect. Technol. Methods* **1**, 15 (2017); P. Cao *et al.*, *Nucl. Instrum. Methods Phys. Res., Sect. A* **953**, 163053 (2020).
- [49] S. Agostinelli *et al.* (GEANT4 Collaboration), *Nucl. Instrum. Methods Phys. Res., Sect. A* **506**, 250 (2003).
- [50] K. X. Huang *et al.*, *Nucl. Sci. Tech.* **33**, 142 (2022).
- [51] S. Jadach, B. F. L. Ward, and Z. Was, *Phys. Rev. D* **63**, 113009 (2001); *Comput. Phys. Commun.* **130**, 260 (2000).
- [52] D. J. Lange, *Nucl. Instrum. Methods Phys. Res., Sect. A* **462**, 152 (2001); R. G. Ping, *Chin. Phys. C* **32**, 599 (2008).
- [53] J. C. Chen, G. S. Huang, X. R. Qi, D. H. Zhang, and Y. S. Zhu, *Phys. Rev. D* **62**, 034003 (2000); R. L. Yang, R. G. Ping, and H. Chen, *Chin. Phys. Lett.* **31**, 061301 (2014).
- [54] E. Richter-Was, *Phys. Lett. B* **303**, 163 (1993).
- [55] M. He, *J. Phys. Conf. Ser.* **293**, 012025 (2011).
- [56] M. Williams, M. Bellis, and C. A. Meyer, *J. Instrum.* **4**, P10003 (2009).
- [57] M. Ablikim *et al.* (BESIII Collaboration), *Phys. Lett. B* **607**, 243 (2005).
- [58] B. Liu, X. Xiong, G. Y. Hou, S. M. Song, and L. Shen, *EPJ Web Conf.* **214**, 06033 (2019).
- [59] N. Berger, B. Liu, and J. Wang, *J. Phys. Conf. Ser.* **219**, 042031 (2010).
- [60] S. Dulat and B. S. Zou, *Eur. Phys. J. A* **26**, 125 (2005).
- [61] M. Ablikim *et al.* (BESIII Collaboration), *Phys. Rev. D* **93**, 112011 (2016).
- [62] F. James and M. Roos, *Comput. Phys. Commun.* **10**, 343 (1975).
- [63] C. Robert and G. Casella, *Technometrics* **47**, 243 (2005).
- [64] J. S. Liu, *Monte Carlo Strategies in Scientific Computing* (Springer, New York, 2001).

- [65] C. Langenbruch, *Eur. Phys. J. C* **82**, 393 (2022).
 [66] M. Ablikim *et al.* (BESIII Collaboration), *Phys. Rev. D* **95**, 032002 (2017).
 [67] M. Ablikim *et al.* (BESIII Collaboration), *Phys. Rev. D* **83**, 112005 (2011).
 [68] M. Ablikim *et al.* (BESIII Collaboration), *Phys. Rev. D* **81**, 052005 (2010).
 [69] M. Ablikim *et al.* (BESIII Collaboration), *Phys. Rev. D* **87**, 012002 (2013).
 [70] D. Y. Chen, Y. B. Dong, and X. Liu, *Eur. Phys. J. C* **70**, 177 (2010).
 [71] Y. G. Gao, Y. J. Zhang, and K. T. Chao, *Chin. Phys. Lett.* **23**, 2376 (2006).
 [72] Stephen R. Cotanch and Robert A. Williams, *Phys. Lett. B* **621**, 269 (2005).
 [73] Y. Chen and Q. Zhao, *Phys. Rev. D* **105**, 076023 (2022).

M. Ablikim,¹ M. N. Achasov,^{5,b} P. Adlarson,⁷⁴ X. C. Ai,⁸⁰ R. Aliberti,³⁵ A. Amoroso,^{73a,73c} M. R. An,³⁹ Q. An,^{70,57} Y. Bai,⁵⁶ O. Bakina,³⁶ I. Balossino,^{29a} Y. Ban,^{46,g} V. Batozskaya,^{1,44} K. Begzsuren,³² N. Berger,³⁵ M. Berlowski,⁴⁴ M. Bertani,^{28a} D. Bettoni,^{29a} F. Bianchi,^{73a,73c} E. Bianco,^{73a,73c} A. Bortone,^{73a,73c} I. Boyko,³⁶ R. A. Briere,⁶ A. Brueggemann,⁶⁷ H. Cai,⁷⁵ X. Cai,^{1,57} A. Calcaterra,^{28a} G. F. Cao,^{1,62} N. Cao,^{1,62} S. A. Cetin,^{61a} J. F. Chang,^{1,57} T. T. Chang,⁷⁶ W. L. Chang,^{1,62} G. R. Che,⁴³ G. Chelkov,^{36,a} C. Chen,⁴³ Chao Chen,⁵⁴ G. Chen,¹ H. S. Chen,^{1,62} M. L. Chen,^{1,57,62} S. J. Chen,⁴² S. M. Chen,⁶⁰ T. Chen,^{1,62} X. R. Chen,^{31,62} X. T. Chen,^{1,62} Y. B. Chen,^{1,57} Y. Q. Chen,³⁴ Z. J. Chen,^{25,h} W. S. Cheng,^{73c} S. K. Choi,¹¹ X. Chu,⁴³ G. Cibinetto,^{29a} S. C. Coen,⁴ F. Cossio,^{73c} J. J. Cui,⁴⁹ H. L. Dai,^{1,57} J. P. Dai,⁷⁸ A. Dbeyssi,¹⁸ R. E. de Boer,⁴ D. Dedovich,³⁶ Z. Y. Deng,¹ A. Denig,³⁵ I. Denysenko,³⁶ M. Destefanis,^{73a,73c} F. De Mori,^{73a,73c} B. Ding,^{65,1} X. X. Ding,^{46,g} Y. Ding,⁴⁰ Y. Ding,³⁴ J. Dong,^{1,57} L. Y. Dong,^{1,62} M. Y. Dong,^{1,57,62} X. Dong,⁷⁵ M. C. Du,¹ S. X. Du,⁸⁰ Z. H. Duan,⁴² P. Egorov,^{36,a} Y. H. Y. Fan,⁴⁵ Y. L. Fan,⁷⁵ J. Fang,^{1,57} S. S. Fang,^{1,62} W. X. Fang,¹ Y. Fang,¹ R. Farinelli,^{29a} L. Fava,^{73b,73c} F. Feldbauer,⁴ G. Felici,^{28a} C. Q. Feng,^{70,57} J. H. Feng,⁵⁸ K. Fischer,⁶⁸ M. Fritsch,⁴ C. Fritsch,⁶⁷ C. D. Fu,¹ J. L. Fu,⁶² Y. W. Fu,¹ H. Gao,⁶² Y. N. Gao,^{46,g} Yang Gao,^{70,57} S. Garbolino,^{73c} I. Garzia,^{29a,29b} P. T. Ge,⁷⁵ Z. W. Ge,⁴² C. Geng,⁵⁸ E. M. Gersabeck,⁶⁶ A. Gilman,⁶⁸ K. Goetzen,¹⁴ L. Gong,⁴⁰ W. X. Gong,^{1,57} W. Gradl,³⁵ S. Gramigna,^{29a,29b} M. Greco,^{73a,73c} M. H. Gu,^{1,57} C. Y. Guan,^{1,62} Z. L. Guan,²² A. Q. Guo,^{31,62} L. B. Guo,⁴¹ M. J. Guo,⁴⁹ R. P. Guo,⁴⁸ Y. P. Guo,^{13,f} A. Guskov,^{36,a} T. T. Han,¹ W. Y. Han,³⁹ X. Q. Hao,¹⁹ F. A. Harris,⁶⁴ K. K. He,⁵⁴ K. L. He,^{1,62} F. H. H. Heinsius,⁴ C. H. Heinz,³⁵ Y. K. Heng,^{1,57,62} C. Herold,⁵⁹ T. Holtmann,⁴ P. C. Hong,^{13,f} G. Y. Hou,^{1,62} X. T. Hou,^{1,62} Y. R. Hou,⁶² Z. L. Hou,¹ H. M. Hu,^{1,62} J. F. Hu,^{55,i} T. Hu,^{1,57,62} Y. Hu,¹ G. S. Huang,^{70,57} K. X. Huang,⁵⁸ L. Q. Huang,^{31,62} X. T. Huang,⁴⁹ Y. P. Huang,¹ T. Hussain,⁷² N. Hüsken,^{27,35} W. Imoehl,²⁷ J. Jackson,²⁷ S. Jaeger,⁴ S. Janchiv,³² J. H. Jeong,¹¹ Q. Ji,¹ Q. P. Ji,¹⁹ X. B. Ji,^{1,62} X. L. Ji,^{1,57} Y. Y. Ji,⁴⁹ X. Q. Jia,⁴⁹ Z. K. Jia,^{70,57} H. J. Jiang,⁷⁵ P. C. Jiang,^{46,g} S. S. Jiang,³⁹ T. J. Jiang,¹⁶ X. S. Jiang,^{1,57,62} Y. Jiang,⁶² J. B. Jiao,⁴⁹ Z. Jiao,²³ S. Jin,⁴² Y. Jin,⁶⁵ M. Q. Jing,^{1,62} T. Johansson,⁷⁴ X. Kui,¹ S. Kabana,³³ N. Kalantar-Nayestanaki,⁶³ X. L. Kang,¹⁰ X. S. Kang,⁴⁰ M. Kavatsyuk,⁶³ B. C. Ke,⁸⁰ A. Khoukaz,⁶⁷ R. Kiuchi,¹ R. Kliemt,¹⁴ O. B. Kolcu,^{61a} B. Kopf,⁴ M. Kuessner,⁴ A. Kupsc,^{44,74} W. Kühn,³⁷ J. J. Lane,⁶⁶ P. Larin,¹⁸ A. Lavania,²⁶ L. Lavezzi,^{73a,73c} T. T. Lei,^{70,57} Z. H. Lei,^{70,57} H. Leithoff,³⁵ M. Lellmann,³⁵ T. Lenz,³⁵ C. Li,⁴³ C. Li,⁴⁷ C. H. Li,³⁹ Cheng Li,^{70,57} D. M. Li,⁸⁰ F. Li,^{1,57} G. Li,¹ H. Li,^{70,57} H. B. Li,^{1,62} H. J. Li,¹⁹ H. N. Li,^{55,i} Hui Li,⁴³ J. R. Li,⁶⁰ J. S. Li,⁵⁸ J. W. Li,⁴⁹ K. L. Li,¹⁹ Ke Li,¹ L. J. Li,^{1,62} L. K. Li,¹ Lei Li,³ M. H. Li,⁴³ P. R. Li,^{38,j,k} Q. X. Li,⁴⁹ S. X. Li,¹³ T. Li,⁴⁹ W. D. Li,^{1,62} W. G. Li,¹ X. H. Li,^{70,57} X. L. Li,⁴⁹ Xiaoyu Li,^{1,62} Y. G. Li,^{46,g} Z. J. Li,⁵⁸ C. Liang,⁴² H. Liang,³⁴ H. Liang,^{1,62} H. Liang,^{70,57} Y. F. Liang,⁵³ Y. T. Liang,^{31,62} G. R. Liao,¹⁵ L. Z. Liao,⁴⁹ Y. P. Liao,^{1,62} J. Libby,²⁶ A. Limphirat,⁵⁹ D. X. Lin,^{31,62} T. Lin,¹ B. J. Liu,¹ B. X. Liu,⁷⁵ C. Liu,³⁴ C. X. Liu,¹ F. H. Liu,⁵² Fang Liu,⁷ G. M. Liu,^{55,i} H. Liu,^{38,j,k} H. M. Liu,^{1,62} Huanhuan Liu,¹ Huihui Liu,²¹ J. B. Liu,^{70,57} J. L. Liu,⁷¹ J. Y. Liu,^{1,62} K. Liu,¹ K. Y. Liu,⁴⁰ Ke Liu,²² L. Liu,^{70,57} L. C. Liu,⁴³ Lu Liu,⁴³ M. H. Liu,^{13,f} P. L. Liu,¹ Q. Liu,⁶² S. B. Liu,^{70,57} T. Liu,^{13,f} W. K. Liu,⁴³ W. M. Liu,^{70,57} X. Liu,^{38,j,k} Y. Liu,^{38,j,k} Y. Liu,⁸⁰ Y. B. Liu,⁴³ Z. A. Liu,^{1,57,62} Z. Q. Liu,⁴⁹ X. C. Lou,^{1,57,62} F. X. Lu,⁵⁸ H. J. Lu,²³ J. G. Lu,^{1,57} X. L. Lu,¹ Y. Lu,⁸ Y. P. Lu,^{1,57} Z. H. Lu,^{1,62} C. L. Luo,⁴¹ M. X. Luo,⁷⁹ T. Luo,^{13,f} X. L. Luo,^{1,57} X. R. Lyu,⁶² Y. F. Lyu,⁴³ F. C. Ma,⁴⁰ H. L. Ma,¹ J. L. Ma,^{1,62} L. L. Ma,⁴⁹ M. M. Ma,^{1,62} Q. M. Ma,¹ R. Q. Ma,^{1,62} R. T. Ma,⁶² X. Y. Ma,^{1,57} Y. Ma,^{46,g} Y. M. Ma,³¹ F. E. Maas,¹⁸ M. Maggiora,^{73a,73c} S. Malde,⁶⁸ Q. A. Malik,⁷² A. Mangoni,^{28b} Y. J. Mao,^{46,g} Z. P. Mao,¹ S. Marcello,^{73a,73c} Z. X. Meng,⁶⁵ J. G. Messchendorp,^{14,63} G. Mezzadri,^{29a} H. Miao,^{1,62} T. J. Min,⁴² R. E. Mitchell,²⁷ X. H. Mo,^{1,57,62} N. Yu. Muchnoi,^{5,b} J. Muskalla,³⁵ Y. Nefedov,³⁶ F. Nerling,^{18,d} I. B. Nikolaev,^{5,b} Z. Ning,^{1,57} S. Nisar,^{12,1} Y. Niu,⁴⁹ S. L. Olsen,⁶² Q. Ouyang,^{1,57,62} S. Pacetti,^{28b,28c} X. Pan,⁵⁴ Y. Pan,⁵⁶ A. Pathak,³⁴ P. Patteri,^{28a} Y. P. Pei,^{70,57} M. Pelizaeus,⁴ H. P. Peng,^{70,57} K. Peters,^{14,d} J. L. Ping,⁴¹ R. G. Ping,^{1,62} S. Plura,³⁵ S. Pogodin,³⁶ V. Prasad,³³ F. Z. Qi,¹ H. Qi,^{70,57} H. R. Qi,⁶⁰ M. Qi,⁴²

T. Y. Qi,^{13,f} S. Qian,^{1,57} W. B. Qian,⁶² C. F. Qiao,⁶² J. J. Qin,⁷¹ L. Q. Qin,¹⁵ X. P. Qin,^{13,f} X. S. Qin,⁴⁹ Z. H. Qin,^{1,57} J. F. Qiu,¹ S. Q. Qu,⁶⁰ C. F. Redmer,³⁵ K. J. Ren,³⁹ A. Rivetti,^{73c} M. Rolo,^{73c} G. Rong,^{1,62} Ch. Rosner,¹⁸ S. N. Ruan,⁴³ N. Salone,⁴⁴ A. Sarantsev,^{36,c} Y. Schelhaas,³⁵ K. Schoenning,⁷⁴ M. Scodreggio,^{29a,29b} K. Y. Shan,^{13,f} W. Shan,²⁴ X. Y. Shan,^{70,57} J. F. Shangguan,⁵⁴ L. G. Shao,^{1,62} M. Shao,^{70,57} C. P. Shen,^{13,f} H. F. Shen,^{1,62} W. H. Shen,⁶² X. Y. Shen,^{1,62} B. A. Shi,⁶² H. C. Shi,^{70,57} J. L. Shi,¹³ J. Y. Shi,¹ Q. Q. Shi,⁵⁴ R. S. Shi,^{1,62} X. Shi,^{1,57} J. J. Song,¹⁹ T. Z. Song,⁵⁸ W. M. Song,^{34,1} Y. J. Song,¹³ Y. X. Song,^{46,g} S. Sosio,^{73a,73c} S. Spataro,^{73a,73c} F. Stieler,³⁵ Y. J. Su,⁶² G. B. Sun,⁷⁵ G. X. Sun,¹ H. Sun,⁶² H. K. Sun,¹ J. F. Sun,¹⁹ K. Sun,⁶⁰ L. Sun,⁷⁵ S. S. Sun,^{1,62} T. Sun,^{1,62} W. Y. Sun,³⁴ Y. Sun,¹⁰ Y. J. Sun,^{70,57} Y. Z. Sun,¹ Z. T. Sun,⁴⁹ Y. X. Tan,^{70,57} C. J. Tang,⁵³ G. Y. Tang,¹ J. Tang,⁵⁸ Y. A. Tang,⁷⁵ L. Y. Tao,⁷¹ Q. T. Tao,^{25,h} M. Tat,⁶⁸ J. X. Teng,^{70,57} V. Thoren,⁷⁴ W. H. Tian,⁵¹ W. H. Tian,⁵⁸ Y. Tian,^{31,62} Z. F. Tian,⁷⁵ I. Uman,^{61b} S. J. Wang,⁴⁹ B. Wang,¹ B. L. Wang,⁶² Bo Wang,^{70,57} C. W. Wang,⁴² D. Y. Wang,^{46,g} F. Wang,⁷¹ H. J. Wang,^{38,j,k} H. P. Wang,^{1,62} J. P. Wang,⁴⁹ K. Wang,^{1,57} L. L. Wang,¹ M. Wang,⁴⁹ Meng Wang,^{1,62} S. Wang,^{13,f} S. Wang,^{38,j,k} T. Wang,^{13,f} T. J. Wang,⁴³ W. Wang,⁵⁸ W. Wang,⁷¹ W. P. Wang,^{70,57} X. Wang,^{46,g} X. F. Wang,^{38,j,k} X. J. Wang,³⁹ X. L. Wang,^{13,f} Y. Wang,⁶⁰ Y. D. Wang,⁴⁵ Y. F. Wang,^{1,57,62} Y. H. Wang,⁴⁷ Y. N. Wang,⁴⁵ Y. Q. Wang,¹ Yaqian Wang,^{17,1} Yi Wang,⁶⁰ Z. Wang,^{1,57} Z. L. Wang,⁷¹ Z. Y. Wang,^{1,62} Ziyi Wang,⁶² D. Wei,⁶⁹ D. H. Wei,¹⁵ F. Weidner,⁶⁷ S. P. Wen,¹ C. W. Wenzel,⁴ U. Wiedner,⁴ G. Wilkinson,⁶⁸ M. Wolke,⁷⁴ L. Wollenberg,⁴ C. Wu,³⁹ J. F. Wu,^{1,62} L. H. Wu,¹ L. J. Wu,^{1,62} X. Wu,^{13,f} X. H. Wu,³⁴ Y. Wu,⁷⁰ Y. J. Wu,³¹ Z. Wu,^{1,57} L. Xia,^{70,57} X. M. Xian,³⁹ T. Xiang,^{46,g} D. Xiao,^{38,j,k} G. Y. Xiao,⁴² S. Y. Xiao,¹ Y. L. Xiao,^{13,f} Z. J. Xiao,⁴¹ C. Xie,⁴² X. H. Xie,^{46,g} Y. Xie,⁴⁹ Y. G. Xie,^{1,57} Y. H. Xie,⁷ Z. P. Xie,^{70,57} T. Y. Xing,^{1,62} C. F. Xu,^{1,62} C. J. Xu,⁵⁸ G. F. Xu,¹ H. Y. Xu,⁶⁵ Q. J. Xu,¹⁶ Q. N. Xu,³⁰ W. Xu,^{1,62} W. L. Xu,⁶⁵ X. P. Xu,⁵⁴ Y. C. Xu,⁷⁷ Z. P. Xu,⁴² Z. S. Xu,⁶² F. Yan,⁴² L. Yan,^{13,f} W. B. Yan,^{70,57} W. C. Yan,⁸⁰ X. Q. Yan,¹ H. J. Yang,^{50,e} H. L. Yang,³⁴ H. X. Yang,¹ Tao Yang,¹ Y. Yang,^{13,f} Y. F. Yang,⁴³ Y. X. Yang,^{1,62} Yifan Yang,^{1,62} Z. W. Yang,^{38,j,k} Z. P. Yao,⁴⁹ M. Ye,^{1,57} M. H. Ye,⁹ J. H. Yin,¹ Z. Y. You,⁵⁸ B. X. Yu,^{1,57,62} C. X. Yu,⁴³ G. Yu,^{1,62} J. S. Yu,^{25,h} T. Yu,⁷¹ X. D. Yu,^{46,g} C. Z. Yuan,^{1,62} L. Yuan,² S. C. Yuan,¹ X. Q. Yuan,¹ Y. Yuan,^{1,62} Z. Y. Yuan,⁵⁸ C. X. Yue,³⁹ A. A. Zafar,⁷² F. R. Zeng,⁴⁹ X. Zeng,^{13,f} Y. Zeng,^{25,h} Y. J. Zeng,^{1,62} X. Y. Zhai,³⁴ Y. C. Zhai,⁴⁹ Y. H. Zhan,⁵⁸ A. Q. Zhang,^{1,62} B. L. Zhang,^{1,62} B. X. Zhang,¹ D. H. Zhang,⁴³ G. Y. Zhang,¹⁹ H. Zhang,⁷⁰ H. H. Zhang,⁵⁸ H. H. Zhang,³⁴ H. Q. Zhang,^{1,57,62} H. Y. Zhang,^{1,57} J. Zhang,⁸⁰ J. J. Zhang,⁵¹ J. L. Zhang,²⁰ J. Q. Zhang,⁴¹ J. W. Zhang,^{1,57,62} J. X. Zhang,^{38,j,k} J. Y. Zhang,¹ J. Z. Zhang,^{1,62} Jianyu Zhang,⁶² Jiawei Zhang,^{1,62} L. M. Zhang,⁶⁰ L. Q. Zhang,⁵⁸ Lei Zhang,⁴² P. Zhang,^{1,62} Q. Y. Zhang,^{39,80} Shuihan Zhang,^{1,62} Shulei Zhang,^{25,h} X. D. Zhang,⁴⁵ X. M. Zhang,¹ X. Y. Zhang,⁴⁹ Xuyan Zhang,⁵⁴ Y. Zhang,⁷¹ Y. Zhang,⁶⁸ Y. T. Zhang,⁸⁰ Y. H. Zhang,^{1,57} Yan Zhang,^{70,57} Yao Zhang,¹ Z. H. Zhang,¹ Z. L. Zhang,³⁴ Z. Y. Zhang,⁷⁵ Z. Y. Zhang,⁴³ G. Zhao,¹ J. Zhao,³⁹ J. Y. Zhao,^{1,62} J. Z. Zhao,^{1,57} Lei Zhao,^{70,57} Ling Zhao,¹ M. G. Zhao,⁴³ S. J. Zhao,⁸⁰ Y. B. Zhao,^{1,57} Y. X. Zhao,^{31,62} Z. G. Zhao,^{70,57} A. Zhemchugov,^{36,a} B. Zheng,⁷¹ J. P. Zheng,^{1,57} W. J. Zheng,^{1,62} Y. H. Zheng,⁶² B. Zhong,⁴¹ X. Zhong,⁵⁸ H. Zhou,⁴⁹ L. P. Zhou,^{1,62} X. Zhou,⁷⁵ X. K. Zhou,⁷ X. R. Zhou,^{70,57} X. Y. Zhou,³⁹ Y. Z. Zhou,^{13,f} J. Zhu,⁴³ K. Zhu,¹ K. J. Zhu,^{1,57,62} L. Zhu,³⁴ L. X. Zhu,⁶² S. H. Zhu,⁶⁹ S. Q. Zhu,⁴² T. J. Zhu,^{13,f} W. J. Zhu,^{13,f} Y. C. Zhu,^{70,57} Z. A. Zhu,^{1,62} J. H. Zou,¹ and J. Zu^{70,57}

(BESIII Collaboration)

¹*Institute of High Energy Physics, Beijing 100049, People's Republic of China*²*Beihang University, Beijing 100191, People's Republic of China*³*Beijing Institute of Petrochemical Technology, Beijing 102617, People's Republic of China*⁴*Bochum Ruhr-University, D-44780 Bochum, Germany*⁵*Budker Institute of Nuclear Physics SB RAS (BINP), Novosibirsk 630090, Russia*⁶*Carnegie Mellon University, Pittsburgh, Pennsylvania 15213, USA*⁷*Central China Normal University, Wuhan 430079, People's Republic of China*⁸*Central South University, Changsha 410083, People's Republic of China*⁹*China Center of Advanced Science and Technology, Beijing 100190, People's Republic of China*¹⁰*China University of Geosciences, Wuhan 430074, People's Republic of China*¹¹*Chung-Ang University, Seoul, 06974, Republic of Korea*¹²*COMSATS University Islamabad, Lahore Campus, Defence Road, Off Raiwind Road, 54000 Lahore, Pakistan*¹³*Fudan University, Shanghai 200433, People's Republic of China*¹⁴*GSI Helmholtzcentre for Heavy Ion Research GmbH, D-64291 Darmstadt, Germany*¹⁵*Guangxi Normal University, Guilin 541004, People's Republic of China*¹⁶*Hangzhou Normal University, Hangzhou 310036, People's Republic of China*

- ¹⁷Hebei University, Baoding 071002, People's Republic of China
- ¹⁸Helmholtz Institute Mainz, Staudinger Weg 18, D-55099 Mainz, Germany
- ¹⁹Henan Normal University, Xinxiang 453007, People's Republic of China
- ²⁰Henan University, Kaifeng 475004, People's Republic of China
- ²¹Henan University of Science and Technology, Luoyang 471003, People's Republic of China
- ²²Henan University of Technology, Zhengzhou 450001, People's Republic of China
- ²³Huangshan College, Huangshan 245000, People's Republic of China
- ²⁴Hunan Normal University, Changsha 410081, People's Republic of China
- ²⁵Hunan University, Changsha 410082, People's Republic of China
- ²⁶Indian Institute of Technology Madras, Chennai 600036, India
- ²⁷Indiana University, Bloomington, Indiana 47405, USA
- ^{28a}INFN Laboratori Nazionali di Frascati, INFN Laboratori Nazionali di Frascati, I-00044, Frascati, Italy
- ^{28b}INFN Sezione di Perugia, I-06100, Perugia, Italy
- ^{28c}University of Perugia, I-06100, Perugia, Italy
- ^{29a}INFN Sezione di Ferrara, INFN Sezione di Ferrara, I-44122, Ferrara, Italy
- ^{29b}University of Ferrara, I-44122, Ferrara, Italy
- ³⁰Inner Mongolia University, Hohhot 010021, People's Republic of China
- ³¹Institute of Modern Physics, Lanzhou 730000, People's Republic of China
- ³²Institute of Physics and Technology, Peace Avenue 54B, Ulaanbaatar 13330, Mongolia
- ³³Instituto de Alta Investigación, Universidad de Tarapacá, Casilla 7D, Arica 1000000, Chile
- ³⁴Jilin University, Changchun 130012, People's Republic of China
- ³⁵Johannes Gutenberg University of Mainz, Johann-Joachim-Becher-Weg 45, D-55099 Mainz, Germany
- ³⁶Joint Institute for Nuclear Research, 141980 Dubna, Moscow region, Russia
- ³⁷Justus-Liebig-Universität Giessen, II. Physikalisches Institut, Heinrich-Buff-Ring 16, D-35392 Giessen, Germany
- ³⁸Lanzhou University, Lanzhou 730000, People's Republic of China
- ³⁹Liaoning Normal University, Dalian 116029, People's Republic of China
- ⁴⁰Liaoning University, Shenyang 110036, People's Republic of China
- ⁴¹Nanjing Normal University, Nanjing 210023, People's Republic of China
- ⁴²Nanjing University, Nanjing 210093, People's Republic of China
- ⁴³Nankai University, Tianjin 300071, People's Republic of China
- ⁴⁴National Centre for Nuclear Research, Warsaw 02-093, Poland
- ⁴⁵North China Electric Power University, Beijing 102206, People's Republic of China
- ⁴⁶Peking University, Beijing 100871, People's Republic of China
- ⁴⁷Qufu Normal University, Qufu 273165, People's Republic of China
- ⁴⁸Shandong Normal University, Jinan 250014, People's Republic of China
- ⁴⁹Shandong University, Jinan 250100, People's Republic of China
- ⁵⁰Shanghai Jiao Tong University, Shanghai 200240, People's Republic of China
- ⁵¹Shanxi Normal University, Linfen 041004, People's Republic of China
- ⁵²Shanxi University, Taiyuan 030006, People's Republic of China
- ⁵³Sichuan University, Chengdu 610064, People's Republic of China
- ⁵⁴Soochow University, Suzhou 215006, People's Republic of China
- ⁵⁵South China Normal University, Guangzhou 510006, People's Republic of China
- ⁵⁶Southeast University, Nanjing 211100, People's Republic of China
- ⁵⁷State Key Laboratory of Particle Detection and Electronics, Beijing 100049, Hefei 230026, People's Republic of China
- ⁵⁸Sun Yat-Sen University, Guangzhou 510275, People's Republic of China
- ⁵⁹Suranaree University of Technology, University Avenue 111, Nakhon Ratchasima 30000, Thailand
- ⁶⁰Tsinghua University, Beijing 100084, People's Republic of China
- ^{61a}Turkish Accelerator Center Particle Factory Group, Istinye University, 34010, Istanbul, Turkey
- ^{61b}Near East University, Nicosia, North Cyprus, 99138, Mersin 10, Turkey
- ⁶²University of Chinese Academy of Sciences, Beijing 100049, People's Republic of China
- ⁶³University of Groningen, NL-9747 AA Groningen, The Netherlands
- ⁶⁴University of Hawaii, Honolulu, Hawaii 96822, USA
- ⁶⁵University of Jinan, Jinan 250022, People's Republic of China
- ⁶⁶University of Manchester, Oxford Road, Manchester, M13 9PL, United Kingdom
- ⁶⁷University of Muenster, Wilhelm-Klemm-Strasse 9, 48149 Muenster, Germany
- ⁶⁸University of Oxford, Keble Road, Oxford OX13RH, United Kingdom
- ⁶⁹University of Science and Technology Liaoning, Anshan 114051, People's Republic of China
- ⁷⁰University of Science and Technology of China, Hefei 230026, People's Republic of China

- ⁷¹*University of South China, Hengyang 421001, People's Republic of China*
⁷²*University of the Punjab, Lahore-54590, Pakistan*
^{73a}*University of Turin and INFN, University of Turin, I-10125, Turin, Italy*
^{73b}*University of Eastern Piedmont, I-15121, Alessandria, Italy*
^{73c}*INFN, I-10125, Turin, Italy*
⁷⁴*Uppsala University, Box 516, SE-75120 Uppsala, Sweden*
⁷⁵*Wuhan University, Wuhan 430072, People's Republic of China*
⁷⁶*Xinyang Normal University, Xinyang 464000, People's Republic of China*
⁷⁷*Yantai University, Yantai 264005, People's Republic of China*
⁷⁸*Yunnan University, Kunming 650500, People's Republic of China*
⁷⁹*Zhejiang University, Hangzhou 310027, People's Republic of China*
⁸⁰*Zhengzhou University, Zhengzhou 450001, People's Republic of China*

^aAlso at the Moscow Institute of Physics and Technology, Moscow 141700, Russia.

^bAlso at the Novosibirsk State University, Novosibirsk, 630090, Russia.

^cAlso at the NRC "Kurchatov Institute," PNPI, 188300, Gatchina, Russia.

^dAlso at Goethe University Frankfurt, 60323 Frankfurt am Main, Germany.

^eAlso at Key Laboratory for Particle Physics, Astrophysics and Cosmology, Ministry of Education; Shanghai Key Laboratory for Particle Physics and Cosmology; Institute of Nuclear and Particle Physics, Shanghai 200240, People's Republic of China.

^fAlso at Key Laboratory of Nuclear Physics and Ion-beam Application (MOE) and Institute of Modern Physics, Fudan University, Shanghai 200443, People's Republic of China.

^gAlso at State Key Laboratory of Nuclear Physics and Technology, Peking University, Beijing 100871, People's Republic of China.

^hAlso at School of Physics and Electronics, Hunan University, Changsha 410082, China.

ⁱAlso at Guangdong Provincial Key Laboratory of Nuclear Science, Institute of Quantum Matter, South China Normal University, Guangzhou 510006, China.

^jAlso at Frontiers Science Center for Rare Isotopes, Lanzhou University, Lanzhou 730000, People's Republic of China.

^kAlso at Lanzhou Center for Theoretical Physics, Lanzhou University, Lanzhou 730000, People's Republic of China.

^lAlso at the Department of Mathematical Sciences, IBA, Karachi 75270, Pakistan.